Merve Begum Terzi* and Orhan Arikan

Machine learning based hybrid anomaly detection technique for automatic diagnosis of cardiovascular diseases using cardiac sympathetic nerve activity and electrocardiogram

https://doi.org/10.1515/bmt-2022-0406
Received October 19, 2022; accepted August 25, 2023;
published online October 12, 2023

Abstract

Objectives: Coronary artery diseases (CADs) are the leading cause of death worldwide and early diagnosis is crucial for timely treatment. To address this, our study presents a novel automated Artificial Intelligence (AI)-based Hybrid Anomaly Detection (AIHAD) technique that combines various signal processing, feature extraction, supervised, and unsupervised machine learning methods. By jointly and simultaneously analyzing 12-lead cardiac sympathetic nerve activity (CSNA) and electrocardiogram (ECG) data, the automated AIHAD technique performs fast, early, and accurate diagnosis of CADs.

Methods: In order to develop and evaluate the proposed automated AIHAD technique, we utilized the fully labeled STAFF III and PTBD databases, which contain the 12-lead wideband raw recordings non-invasively acquired from 260 subjects. Using these wideband raw recordings, we developed a signal processing technique that simultaneously detects the 12-lead CSNA and ECG signals of all subjects. Using the pre-processed 12-lead CSNA and ECG signals, we developed a time-domain feature extraction technique that extracts the statistical CSNA and ECG features critical for the reliable diagnosis of CADs. Using the extracted discriminative features, we developed a supervised classification technique based on Artificial Neural Networks (ANNs) that simultaneously detects anomalies in the 12-lead CSNA and ECG data. Furthermore, we developed an unsupervised clustering technique based on Gaussian mixture models (GMMs) and Neyman-Pearson criterion, which robustly detects outliers corresponding to CADs.

Results: Using the automated AIHAD technique, we have, for the first time, demonstrated a significant association between the increase in CSNA signals and anomalies in ECG signals during CADs. The AIHAD technique achieved highly reliable detection of CADs with a sensitivity of 98.48 %, specificity of 97.73 %, accuracy of 98.11 %, positive predictive value of 97.74 %, negative predictive value of 98.47 %, and F1-score of 98.11 %. Hence, the automated AIHAD technique demonstrates superior performance compared to the gold standard diagnostic test ECG in the diagnosis of CADs. Additionally, it outperforms other techniques developed in this study that separately utilize either only CSNA data or only ECG data. Therefore, it significantly increases the detection performance of CADs by taking advantage of the diversity in different data types and leveraging their strengths. Furthermore, its performance is comparatively better than that of most previously proposed machine and deep learning methods that exclusively used ECG data to diagnose or classify CADs. Additionally, it has a very low implementation time, which is highly desirable for real-time detection of CADs.

Conclusions: The proposed automated AIHAD technique may serve as an efficient decision-support system to increase physicians' success in fast, early, and accurate diagnosis of CADs. It may be highly beneficial and valuable, particularly for asymptomatic patients, for whom the diagnostic information provided by ECG alone is not sufficient to reliably diagnose the disease. Hence, it may significantly improve patient outcomes by enabling timely treatments and considerably reducing the mortality of cardiovascular diseases (CVDs).

Keywords: signal processing; feature extraction; classification; clustering; synthetic minority oversampling technique (SMOTE); Neyman-Pearson hypothesis testing

***Corresponding author: Merve Begum Terzi**, Faculty of Engineering, Electrical and Electronics Engineering Department, Bilkent University, 06800, Ankara, Türkiye, E-mail: mervebegumterzi@gmail.com. https://orcid.org/0000-0002-8680-3781

Orhan Arikan, Faculty of Engineering, Electrical and Electronics Engineering Department, Bilkent University, Ankara, Türkiye

Introduction

According to the World Health Organization (WHO), cardiovascular diseases (CVDs) are the leading cause of death worldwide, with an estimated death rate of approximately 17.9 million deaths each year, accounting for 31 % of all deaths worldwide annually [1]. The majority of these deaths are caused by coronary artery diseases (CADs), including myocardial ischemia (ISC), silent (asymptomatic) myocardial ischemia (AISC), and myocardial infarction (MI, heart attack).

In patients with CADs, significant anomalies in the ST segment, QRS complex, and T wave of the electrocardiogram (ECG) signals occur during ISC and MI [2–6]. However, a considerable number of CAD patients worldwide suffer from AISC, in which there are no anomalies in patients' ECG signals. Thus, an ECG signal that does not contain any anomalies does not rule out the possibility of CADs. Due to its limitations in diagnosing asymptomatic CAD patients with AISC, ECG alone cannot be used to diagnose AISC based solely on its diagnostic information. Since asymptomatic CAD patients with AISC do not experience any symptoms, they are prone to misinterpretation by cardiologists, which leads to false-negative results, making AISC more dangerous and fatal.

Moreover, previous artificial intelligence (AI) studies that exclusively used ECG data to diagnose or classify CADs may have significant limitations for asymptomatic CAD patients with AISC [3, 7–12]. Thus, an automated AI technique that can accurately and quickly diagnose both asymptomatic CAD patients (AISC) and symptomatic CAD patients (ISC, MI) is a major and essential clinical need that may significantly increase the detection performance of CVDs, provide timely treatment, and reduce mortality rates.

Previous studies have shown that the sympathetic nervous system (SNS) plays an important role in regulating the cardiovascular system [13–15]. These studies have established a direct and strong relationship between the SNS and various CVDs, which is due to the fact that the extensions of the SNS that regulate the heart are distributed throughout the heart. The traditional method for directly recording and monitoring high-frequency signals, including activities of the SNS, is the microneurography technique, which requires invasive procedures, such as inserting very fine microelectrodes into the nerve fibers to detect and measure their electrical signals [13, 14, 16]. However, the invasive and complex nature of the microneurography technique, which requires highly specialized expertise from trained clinicians, greatly limits its utilization for research studies in clinical practice.

Recent studies have shown that it is possible to non-invasively record high-frequency signals, called cardiac sympathetic nerve activity (CSNA), from the skin surface of the chest using data acquisition equipment with wide frequency bandwidth and high sampling rate [13, 14, 16]. A few studies investigating the relationship between CSNA and cardiac arrhythmias (CARs) using signal processing techniques demonstrated an increase in the amplitude of CSNA during CARs [14, 16]. Additionally, they indicated that this increase in CSNA was accompanied by a simultaneous increase in heart rate in the ECG signal. Therefore, they suggested that early and reliable diagnosis of CARs can be achieved by detecting the anomalies in CSNA. However, none of these previous studies used AI techniques to diagnose CARs using only CSNA data or both CSNA and ECG data.

Since it has long been accepted that there is a direct and strong relationship between the SNS and various CVDs [13–15], we hypothesized that there can be anomalies in CSNA during CADs. To the best of our knowledge, there are no studies in the literature to date that have investigated whether there is an association between CSNA and CADs using AI techniques. This constituted a research gap in the literature that highlights the need for further investigation. Additionally, most of the existing AI studies have only used ECG data to detect various CVDs. However, there are no studies to date that have proposed an AI technique that jointly and simultaneously uses CSNA and ECG data to diagnose CADs or other CVDs.

The main aim and motivation of this study were to develop an automated AI technique that accurately diagnoses both asymptomatic CAD patients (AISC) and symptomatic CAD patients (ISC, MI) by jointly and simultaneously analyzing 12-lead CSNA and ECG data. Hence, this technique aims to address the limitations of existing related studies that have only used ECG data and fill the research gaps in the literature. For this purpose, we propose a novel AI-based Hybrid Anomaly Detection (AIHAD) technique consisting of various signal processing, feature extraction, supervised, and unsupervised machine learning methods that jointly and simultaneously analyzes 12-lead CSNA and ECG data to perform fast, early, and accurate diagnosis of CADs (i.e., AISC, ISC, MI).

By using the proposed automated AIHAD technique, we aimed to investigate whether there are anomalies in CSNA signals during CADs. Moreover, our purpose was to determine whether the joint and simultaneous detection of the anomalies in the 12-lead CSNA and ECG data provides an increase in the performance of CAD diagnosis. Furthermore, we targeted to compare the performance of the AIHAD technique with the gold standard diagnostic test ECG, as well

as previously proposed AI methods that have only used ECG data to diagnose or classify CADs.

In the literature, various machine and deep learning methods have been previously proposed for the diagnosis and classification of various CVDs using only ECG data. The feature extraction methods can be divided into three groups, which are time-domain techniques, frequency-domain techniques, and time-frequency domain techniques. Specifically, these techniques include Fourier transform [17, 18], wavelet transform [19–30], Gabor transform [31], discrete cosine transform [27], shearlet and contourlet transform [32], Hilbert-Huang transform [33, 34], discrete orthogonal Stockwell transform [35], empirical and variational mode decompositions [26, 27, 34, 36], Wigner-Ville distribution technique [37], Fourier-Bessel series expansion (FBSE) [38–41], and independent and principal component analyses [42, 43].

The previously proposed machine learning methods for the diagnosis and classification of various CVDs using only ECG data include logistic regression [10, 11, 44], artificial neural network (ANN) [10, 19, 25, 37, 45–49], k-nearest neighbor (KNN) [9, 27–29, 32, 39, 48, 50, 51], hidden Markov model (HMM) [22, 52], Gaussian mixture model (GMM) [23, 53], support vector machine (SVM) [8, 10, 17, 20, 24, 35, 36, 41, 48, 50, 53–57], random forest [22, 37, 48, 50, 58, 59], naive Bayes [10, 46, 50, 60], decision tree [4, 21, 32, 46, 60, 61], fuzzy logic [62, 63], self-organizing map (SOM) [64], mixture of experts [65, 66], association rule learning [67], and linear discriminant analysis [50].

Moreover, the previously proposed deep learning methods for the diagnosis and classification of various CVDs using only ECG data include one-dimensional (1D) convolutional neural network (CNN) [3, 12, 42, 68–75], recurrent neural network (RNN) [76–82], combined CNN-RNN [6, 83, 84], capsule network [85], deep neural network (DNN) [26, 86], deep belief network (DBN) [33], autoencoder [54, 64, 78, 87], and restricted Boltzmann machine (RBM) [64, 88]. However, none of these existing machine and deep learning studies have jointly utilized CSNA and ECG data to benefit from the diversity in different data types and to leverage their strengths for the accurate and reliable diagnosis of CVDs.

The main contributions and novelty of the proposed study are summarized as follows:

(1) We developed the first automated AIHAD technique consisting of various signal processing, feature extraction, supervised, and unsupervised machine learning methods that jointly and simultaneously analyze 12-lead CSNA and ECG data to perform fast, early, and accurate diagnosis of CADs.
(2) Our study is the first to demonstrate that there are anomalies in CSNA signals during CADs. Additionally, we have shown that there is a significant association between the increase in CSNA signals and the anomalies in ECG signals during CADs.
(3) The proposed AIHAD technique outperforms other techniques developed in this study that separately use either only CSNA data or only ECG data. Therefore, it significantly increases the detection performance of CADs by benefiting from the diversity in different data types and leveraging their strengths.
(4) The AIHAD technique can automatically process all 12-leads for enhanced diagnosis. Therefore, it takes advantage of the diversity in diagnostic information provided by all 12-leads and can accurately detect CAD cases that cannot be diagnosed using only one-lead.
(5) The automated AIHAD technique demonstrates superior performance compared to the gold standard diagnostic test ECG in the diagnosis of CADs.
(6) The performance of the AIHAD technique is higher than that of most previously proposed machine or deep learning methods that have only used ECG data to diagnose or classify CADs.
(7) The AIHAD technique has a very short implementation time, which is highly desirable for real-time detection of CADs. This may support fast decision-making by physicians in clinical settings, which may have significant implications in emergency situations where rapid diagnosis is crucial for timely patient treatment.

Materials and methods

This study proposes the first automated AIHAD technique consisting of various signal processing, feature extraction, supervised, and unsupervised machine learning methods that jointly and simultaneously analyze 12-lead CSNA and ECG data to perform fast, early, and accurate detection of CADs. The block diagram illustrating the overall structure and methodology of the study is shown in Figure 1. In-depth explanations of the various components and processing steps of the proposed AIHAD technique can be found within the subheadings of the Materials and Methods section.

Data acquisition and preparation

The STAFF III database: One of the databases used for the development and performance evaluation of the proposed automated AIHAD technique is the fully labeled STAFF III database on PhysioNet, which is a publicly available repository of medical research data [89, 90]. The STAFF III database was constructed by acquiring wideband recordings from 104 patients with CADs who underwent percutaneous coronary intervention (PCI) at Charleston Area Medical Center (U.S.). The demographics and clinical characteristics of the patients included in the study are presented in Table 1.

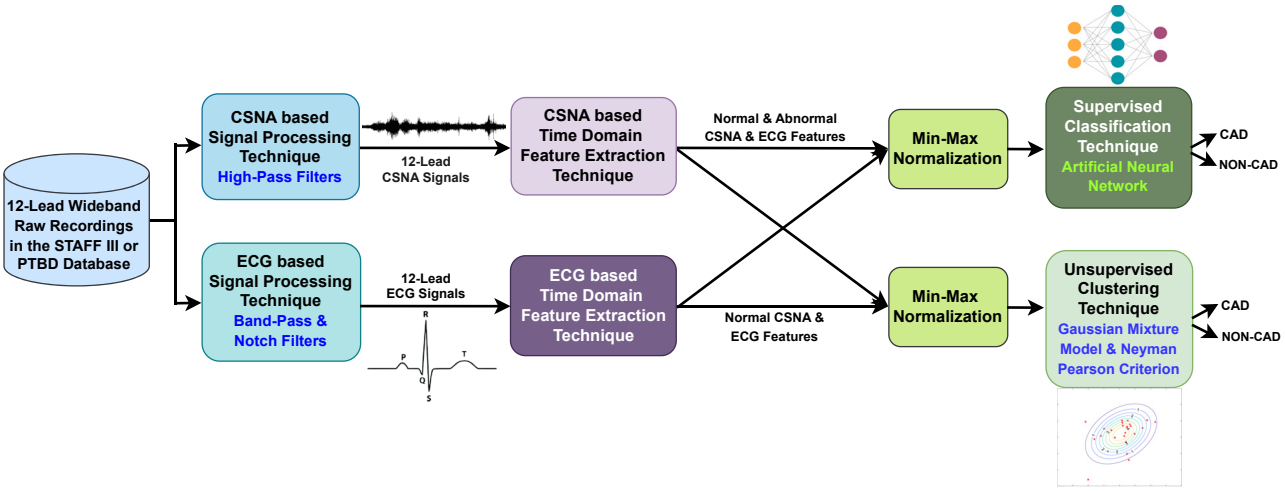

Figure 1: The block diagram that demonstrates various components of the proposed automated AIHAD technique, which are signal processing, feature extraction, supervised classification, and unsupervised clustering methods. The supervised and unsupervised machine learning methods were independently trained with 12-lead CSNA and ECG data, during which they learned to successfully distinguish between patients with and without CADs.

Table 1: The demographics and clinical characteristics of the patients.

Age	55.6 ± 17
Male	65 (62.5 %)
Diabetes	27 (26 %)
Hypertension	43 (41.3 %)
Smoking	33 (31.7 %)

The numerical variables are presented as the mean ± standard deviation. The categorical variables are presented as the number of patients and percentage with respect to the total population.

The database was constructed by Duke University as a part of a clinical research study to investigate high-frequency anomalies in ECG signals that occur during artificially induced ISC caused by complete coronary artery occlusion due to PCI [89, 90]. PCI is a minimally invasive surgical procedure that can cause significant anomalies in the ST segment and T wave of the ECG signal.

Two different types of 12-lead wideband recordings that were acquired before and during PCI from all patients in the STAFF III database were included in this study, as detailed in Table 2. Hence, a total of 1,248 pre-inflation (normal) and 1,248 inflation (abnormal) recordings were utilized to develop and evaluate the proposed AIHAD technique. To date, this database is the largest that simulates high-frequency anomalies in wideband recordings acquired during artificially induced ISC under a PCI-controlled environment. Therefore, it serves as an excellent testbed for developing and evaluating various AI techniques that can diagnose and classify CAD.

Table 2: Two different types of recordings and numbers of the patients and recordings for each type.

Diagnostic Classes	Numbers of the Patients	Numbers of the Recordings	Numbers of the Leads	Total Numbers of the Recordings
Pre-inflation (Normal)	104	104	12	1,248
Inflation (Abnormal)	104	104	12	1,248
Total	104[a]	208	12	2,496

[a]The pre-inflation and inflation recordings belong to the same patients. Therefore, the total number of patients is the same as the number of patients with the pre-inflation or inflation recordings.

Before PCI, the 12-lead pre-inflation (normal) recordings were acquired prior to catheter insertion into the coronary artery at the preoperative room. During PCI, the 12-lead inflation (abnormal) recordings that started before coronary balloon inflation (CBI) and ended after coronary balloon deflation (CBD) were continuously acquired at the cardiac catheterization laboratory (operation room).

The database contains a total of 152 stenoses in the major coronary arteries, distributed as 58 stenoses in the left anterior descendant artery (LAD), 59 stenoses in the right coronary artery (RCA), 32 stenoses in the left circumflex artery (LCX), and 3 stenoses in the left main artery (LM) (Table 3). A total of 35 patients had a previous MI, as determined by ECG criteria defined by the American Heart Association (AHA) [1]. Additionally, the database includes important annotations provided by experienced cardiologists, including the occluded coronary artery in which PCI was performed, the time instants related to CBI and CBD during PCI, the patient's history of previous MI, and the location of previous MI.

The data were acquired using custom-made ECG data acquisition equipment (Siemens–Elema AB, Sweden) with a wider frequency bandwidth and a higher sampling rate compared to conventional ECG devices. The recordings were digitized with a sampling rate of 1,000 Hz, 16-bit sampling resolution, and 0.6 μV amplitude resolution. The patients who suffered from CARs or MI during data acquisition were excluded from the database.

The Physikalisch-Technische Bundesanstalt Diagnostic database: Another database used for the development and performance evaluation of the proposed automated AIHAD technique is the fully labeled Physikalisch-Technische Bundesanstalt (PTB) Diagnostic (PTBD) database on the PhysioNet repository [90–92]. It was constructed by

Table 3: The clinical characteristics of the patients.

Left anterior descendant artery (LAD)	58 (55.8 %)
Right coronary artery (RCA)	59 (56.7 %)
Left circumflex artery (LCX)	32 (30.8 %)
Left main artery (LM)	3 (2.9 %)
Balloon inflation time (second)	263 ± 54
History of previous MI	35 (33.7 %)

The numerical variables are presented as the mean ± standard deviation. The categorical variables are presented as the number of patients and percentage with respect to the total population.

Table 4: The diagnostic classes of the subjects in the PTBD database.

Diagnostic Classes	Number of the Subjects
Healthy Controls	52
Myocardial Infarction (MI)	148
Cardiomyopathy/Heart Failure	18
Bundle Branch Block	15
Dysrhythmia	14
Myocardial Hypertrophy	7
Valvular Heart Disease	6
Myocarditis	4
Miscellaneous	4

Benjamin Franklin University (Berlin, Germany) to investigate high-frequency anomalies in ECG signals of the patients with various CVDs. Among several different diagnostic classes of CVDs present in the PTBD database that are shown in Table 4, the only diagnostic class which is a type of CAD is the MI class.

Since one of the aims of this study was to perform accurate and reliable detection of CADs, we considered the MI patients in the PTBD database as the abnormal class and the healthy controls as the normal class to perform binary classification. Hence, the 12-lead wideband recordings acquired from 52 healthy controls and 104 MI patients, which account for a total of 156 subjects, were included in this study to develop and evaluate the proposed AIHAD technique (Table 5).

Table 5: Two different types of recordings and numbers of the subjects and recordings for each type.

Diagnostic Classes	Numbers of the Subjects	Numbers of the Recordings	Numbers of the Leads	Total Numbers of the Recordings
Healthy Controls (Normal)	52	104[a]	12	1,248
Myocardial Infarction (MI) (Abnormal)	104	104	12	1,248
Total	156	208	12	2,496

[a]The number of the recordings after the implementation of the synthetic minority oversampling technique (SMOTE), which generates new synthetic samples in the minority class (healthy controls).

In order to overcome the class imbalance between the two classes (MI and healthy controls) in the PTBD database and prevent bias towards the majority class (MI), we adjusted the numbers of recordings belonging to each of the two classes to be equal. In order to equate the number of recordings in the minority and majority classes, we employed the synthetic minority oversampling technique (SMOTE) to generate new synthetic samples in the minority class (healthy controls) by interpolating between existing minority class samples and their nearest neighbors. SMOTE created new synthetic samples that resemble the existing minority class samples, while introducing some variations to expand the feature space. Thus, by producing synthetic samples that are representative of the minority class in the training set, the number of samples in the minority class was equalized with that of the majority class. This way, it was ensured that the class distributions were balanced using a data resampling method and both classes had an equal number of recordings (Table 5). This approach guaranteed that the AIHAD technique assigned equal importance to both classes, improved the technique's ability to learn from the minority class, and increased the technique's generalizability. We implemented SMOTE exclusively on the training set, hence it was not applied to the validation or test sets, which ensured a fair performance evaluation of the proposed technique. Consequently, a total of 1,248 normal recordings of 52 healthy controls, and 1,248 abnormal recordings of 104 MI patients were used for the development and evaluation of the proposed AIHAD technique (Table 5). The training of the automated AIHAD technique was performed on the oversampled and balanced training set.

All data were acquired by experienced physicians using data acquisition equipment (PTB prototype recorder, Germany) with a wide frequency bandwidth and high sampling rate. The recordings were digitized with a sampling rate of 1,000 Hz, 16-bit sampling resolution, and 0.5 μV amplitude resolution. They were annotated by experienced physicians to indicate the demographic and clinical information about the patient's age, gender, diagnosis, medical history, coronary artery pathology, ventriculography, and echocardiography. Hence, the database offers an excellent testbed for developing and evaluating various AI techniques that can diagnose and classify CAD.

Enhanced signal processing technique for CSNA and ECG data analysis: The electrical signals obtained from the skin surface of the chest wall contain signals from a wide variety of nerve activities and myocardium [13–16]. Because of the intensive connections between the sympathetic, motor, and sensory nerves in the body, the nerves originating from different sources can activate simultaneously. Thus, the electrical signals acquired from the chest wall ($y_i(t)$) contain raw ECG ($e_i(t)$), cardiac sympathetic nerve activity (CSNA) ($c_i(t)$), motor and sensory nerve activities (MSNA) ($s_i(t)$), and muscle activity (EMG) ($m_i(t)$) (Equation (1)).

$$y_i(t) = e_i(t) + c_i(t) + s_i(t) + m_i(t), \quad i = 1, ., N. \tag{1}$$

In electrical signals acquired from the chest wall, CSNA will be delayed and will decrease in amplitude as it propagates away from its source. This delay and decrease in amplitude can be mathematically modeled by the delay parameter τ_i and the amplitude parameter α_i (Equation (2)).

$$c_i(t) = \alpha_i \; c(t - \tau_i), \quad 0 < \alpha_i < 1 \tag{2}$$

Most of the diagnostic information in ECG resides below 150 Hz, therefore, the AHA recommends a frequency bandwidth of 0.5 Hz–150 Hz for the diagnostic monitoring of ECG [1]. Moreover, the

electromyogram (EMG) is approximately band-limited to 100 Hz, with small amounts of muscle activity occasionally reaching 400 Hz [13]. Therefore, the implementation of a high-pass filter with a cut-off frequency of f_C=150 Hz to the wideband raw recordings acquired from the chest wall will eliminate ECG and EMG to a large extent. The hypothesis of this study, which is based on the previous studies in the literature [13–16], indicates that CSNA is uncorrelated with MSNA, and thus, it is possible to decouple CSNA from MSNA. Therefore, the signal activity obtained as a result of high-pass filtering the electrical signals acquired from the chest wall will mostly originate from CSNA. In cases where the parameters α_i and τ_i are known, CSNA can be estimated as shown in Equation (3).

$$\hat{c}(t) = \frac{\sum_{i=1}^{N} \alpha_i \; y_i(t+\tau_i)}{\sum_{i=1}^{N} \alpha_i^2} \tag{3}$$

We developed two signal processing techniques, which include various digital filtering methods that remove unwanted frequency components from the wideband raw recordings while preserving the diagnostic information within the recordings, to detect the 12-lead CSNA and ECG signals of all subjects in the STAFF III and PTBD databases (Figure 1).

Firstly, we developed and implemented the band-pass and notch filters on the wideband raw recordings in the STAFF III and PTBD databases to detect the 12-lead ECG signals of all subjects. The lowest frequency component of the ECG signal is generally defined by the slowest possible heart rate, which is 40 beats per minute (bpm) [1, 5, 6, 57, 93–95]. Hence, assuming a periodic signal, the lowest frequency component of the ECG signal can be at least 0.67 Hz. Therefore, to enhance the quality of ECG signals by eliminating low-frequency noises, such as baseline wander and respiratory signals, the lower cut-off frequency of the band-pass filter was designed to be f_{L_1}=0.5 Hz.

Moreover, we eliminated the high-frequency noises in ECG signals, such as muscle activity (EMG) and motion artifacts, by designing the band-pass filter to have a higher cut-off frequency of f_{H_1}=150 Hz, which is compatible with the recommendations of the AHA for the diagnostic monitoring of ECG [1].

Furthermore, we eliminated the 60 Hz power-line interference in the STAFF III database by developing notch filters with lower and higher cut-off frequencies of f_{L_2}=59 Hz and f_{H_2}=61 Hz, respectively [94–96]. Similarly, we eliminated the 50 Hz power-line interference in the PTBD database by developing notch filters with lower and higher cut-off frequencies of f_{L_3}=49 Hz and f_{H_3}=51 Hz, respectively.

We developed a QRS complex detection technique that can adapt to the instantaneous changes in ECG signals by setting an adaptive threshold for each patient, which is higher than the P and T waves and lower than the QRS complex in amplitude [5, 6, 57, 94, 95, 97, 98]. By detecting the signal values where the ECG signal amplitude is higher than the predefined threshold, we performed the robust localization of the QRS complexes in the time domain. By using the detected QRS complexes as the reference points, we segmented the ECG signals of all subjects into individual periods, each corresponding to a single heartbeat [12, 52, 87]. Lastly, we determined the isoelectric line, which represents the reference potential level of the measured heart activity for each recorded heartbeat. We then removed the isoelectric line from each ECG period to accurately detect ischemic ECG anomalies.

Secondly, we developed high-pass filters with a cut-off frequency of f_C=150 Hz and we implemented them on the wideband raw recordings in the STAFF III and PTBD databases to detect the 12-lead CSNA signals of all subjects [13, 14, 16]. Moreover, we investigated the performances of various high-pass filters with different cut-off frequencies up to 500 Hz to detect CSNA. The efforts made to optimize the filters' cut-off frequency for displaying CSNA revealed that a high-pass filter with a cut-off frequency of f_C=150 Hz provides a higher amplitude CSNA and better signal-to-noise ratio (SNR), while effectively suppressing ECG signals. Further increases in the cut-off frequency of the filter eliminated EMG signals to a large extent. However, it also resulted in lower amplitude CSNA and worse signal-to-noise ratio (SNR). Therefore, for higher cut-off frequencies of the filter, the specificity of CSNA recording increased. However, a majority of CSNA was filtered out, which reduced the sensitivity of CSNA recording.

Furthermore, we investigated the power ratios of the inflation (abnormal) CSNA (PR_i) across different frequency bands for all patients in the STAFF III and PTBD databases by designing band-pass filters that have 6 consecutive overlapping frequency ranges, as shown in Table 6.

We obtained the power ratio of the inflation (abnormal) CSNA (PR_i) by calculating the ratio of the average inflation CSNA power during PCI (P_{burst}) to the average inflation CSNA power before PCI ($P_{baseline}$), as shown in Equation 4, where $c_i(t)$ denotes the inflation (abnormal) CSNA.

$$PR_i = \frac{P_{burst}}{P_{baseline}} = \frac{\frac{1}{\Delta t_1}\int_{t_2}^{t_3} |c_i(t)|^2 \, dt}{\frac{1}{\Delta t_0}\int_{t_0}^{t_1} |c_i(t)|^2 \, dt}, \quad \Delta t_1 = t_3 - t_2, \quad \Delta t_0 = t_1 - t_0 \tag{4}$$

The experiment results demonstrated that the power ratio of the inflation (abnormal) CSNA (PR_i) was consistently higher for frequency ranges between 150 and 400 Hz (frequency bands between $1 \le i \le 4$) for all patients in the STAFF III and PTBD databases.

Enhanced feature extraction technique

By using the pre-processed 12-lead CSNA and ECG signals in the STAFF III and PTBD databases, we developed a time-domain feature extraction technique that extracts the statistical CSNA and ECG features that are critical for the reliable diagnosis of CADs [19, 28, 29, 42, 97, 99, 100].

Enhanced feature extraction technique for CSNA signals

Number of CSNA peaks: We detected the peaks of the CSNA signals ($p[n]$) by defining an adaptive threshold (ξ) that is specific to the CSNA signal ($c[n]$) of each patient. By identifying signal values at which the amplitude of CSNA was greater than the predefined threshold (ξ) through a sliding time window (N), we performed the time domain localization of CSNA peaks (Equation (5)). We obtained the number of CSNA peaks ($u[n]$) by calculating the summation of CSNA peaks through the sliding time window (N) (Equation (6)).

Table 6: The consecutive overlapping frequency bands and ranges.

Frequency Bands	Frequency Ranges
i=1	150 Hz–250 Hz
i=2	200 Hz–300 Hz
i=3	250 Hz–350 Hz
i=4	300 Hz–400 Hz
i=5	350 Hz–450 Hz
i=6	400 Hz–500 Hz

$$p[n] = \begin{cases} 1, & c[n+k] \geq \xi, \quad k = 0, ., N-1. \\ 0, & c[n+k] < \xi \end{cases} \tag{5}$$

$$u[n] = \sum_{m=0}^{N-1} p[n+m] \tag{6}$$

Average CSNA: We estimated the average voltage of CSNA per sample ($a[n]$) by integrating CSNA signal ($c[n]$) over the sliding time window (N) and dividing the total voltage by the overall number of samples (N) in the same window (Equation (7)).

$$a[n] = \frac{1}{N} \sum_{m=0}^{N-1} |\, c[n+m] \,| \tag{7}$$

Maximum CSNA: We obtained it by calculating the maximum amplitude of CSNA signal ($c[n]$) through the sliding time window (N) (Equation (8)).

$$m[n] = \max_{0 \leq m \leq N-1} (\, c[n+m] \,) \tag{8}$$

Enhanced feature extraction technique for ECG signals

ST segment level: We obtained it by calculating the summation of all signal amplitudes through the ST segment ($q[n]$) and dividing the total voltage by the overall number of samples (L) in the same interval (Equation (9)).

$$s[n] = \frac{1}{L} \sum_{k=0}^{L-1} q[n+k] \tag{9}$$

ST segment slope: ($\hat{\beta}_1$): We estimated it as the slope of the best fitting line ($\hat{q}[n]$) in Equation (11) in terms of least squares to the samples of the ST segment ($q[n]$). We performed this estimation by finding the least squares estimates β_0 and β_1 that minimize the sum of squared residuals in Equation (10).

$$f[\beta_0, \beta_1] = \sum_{k=0}^{L-1} (\, q[n+k] - (\beta_1 w[n+k] + \beta_0))^2 \tag{10}$$

$$\hat{q}[n] = \beta_1 \; w[n] + \beta_0 \tag{11}$$

T wave area: We approximated it by implementing the trapezoidal rule through the samples of the T wave ($v[n]$) (Equation (12)).

$$t[n] = \sum_{k=1}^{M} \frac{(v[n_{k-1}] + v[n_k])}{2} \Delta n_k, \qquad \Delta n_k = \frac{n_k - n_{k-1}}{M} \tag{12}$$

T wave amplitude: We obtained it by locating the maximum or minimum amplitude of the T wave ($v[n]$) in the time domain (Equation (13)).

$$w[n] = \begin{cases} \min\limits_{n_0 \leq n \leq n_M} (v[n]), & v[n] \leq 0 \\ \max\limits_{n_0 \leq n \leq n_M} (v[n]), & v[n] > 0 \end{cases} \tag{13}$$

Supervised classification technique using artificial neural networks

In the literature, ANN is the most preferred machine learning method for the diagnosis or classification of various CVDs by detecting anomalies in ECG data [10, 25, 37, 45, 46, 48, 49]. This preference can be attributed to the various advantages of ANN, including its strong ability to learn and model non-linear complex relationships between the input and output, its robustness to noise, its ability to handle missing or insufficient data, its generalization capability, its remarkable scalability, its ability to perform parallel processing, and its high speed. Additionally, various types of ANNs can be customized to create tailored solutions that address specific tasks required by physicians, which significantly contributes to their superior performance in the detection of CVDs.

Therefore, in this study, we developed a supervised learning method based on ANN that performs simultaneous and robust detection of anomalies in the 12-lead CSNA and ECG data to realize fast, early, and accurate diagnosis of CADs. Firstly, we normalized the 12-lead normal and abnormal CSNA and ECG features using the min-max normalization method to scale the features of different classes in the same range and to ensure that the developed ANN classifier assigns equal importance to data belonging to the two classes (i.e., normal and abnormal). Hence, by bringing all input variables within a standardized range, our aim was to avoid any bias that may arise due to differences in the scales of the features and to guarantee that the ANN classifier can accurately learn from the data, thereby assuring fairness in the classification process.

In order to evaluate the performance of the developed ANN classifier on previously unseen data, we independently and randomly split the whole data in the STAFF III and PTBD databases into non-intersecting training and test sets using the 10-fold cross-validation method, as shown in Tables 7 and 8. Therefore, we randomly partitioned the entire data in each database into 10 equal-sized subsets, where one of these subsets formed the test set that was exclusively used to assess the generalization performance of the ANN classifier. We aggregated the remaining subsets to form the training set, which was used to train the ANN classifier and optimize its (hyper)parameters. The test set remained unexposed during the training of the ANN to ensure an unbiased estimate of the classifier's performance on previously unseen data.

Additionally, we further independently and randomly divided the training sets in the STAFF III and PTBD databases into the training

Table 7: The numbers of the recordings in the training, validation and test sets for the STAFF III database.

Diagnostic Classes	Training Set	Validation Set	Test Set	Total
Pre-inflation (Normal)	840	276	132	1,248
Inflation (Abnormal)	840	276	132	1,248
Total	1,680	552	264	2,496

The numerical variables are presented as the total number of recordings including all 12-leads.

Table 8: The numbers of the recordings in the training, validation and test sets for the PTBD database.

Diagnostic Classes	Training Set	Validation Set	Test Set	Total
Healthy Controls (Normal)	840	276	132	1,248
Myocardial Infarction (Abnormal)	840	276	132	1,248
Total	1,680	552	264	2,496

The numerical variables are presented as the total number of recordings including all 12-leads.

(75 %) and validation (25 %) subsets, as shown in Tables 7 and 8, using the holdout cross-validation method to prevent the ANN classifier from over-fitting to the training sets and ensure better generalization. To guarantee robustness, we repeated this process 10 times for each cross-validation fold, resulting in 10 independent and non-intersecting training, validation, and test subsets that were randomly constituted. Each pattern was used in the test set exactly once in each cross-validation fold to maintain fairness. By taking the average of the statistical performance results calculated across 10 different cross-validation folds, a single estimation that represents the binary classification performance of the optimum ANN classifier for each of the training, validation, and test subsets was independently produced for the STAFF III and PTBD databases. The absence of class imbalance between the two classes in the training and validation sets of both databases prevented bias and over-fitting during training, and allowed the ANN classifier to generalize very well on previously unseen data.

The feed-forward ANN classifier architecture consists of three layers, which are an input layer with seven neurons, a hidden layer, and an output layer with two neurons. The number of neurons in the input layer is equal to the total number of CSNA and ECG features. In order to empirically determine the optimum number of hidden layers, various multilayer perceptrons (MLPs) with single and multiple hidden layers were developed. The experimental results showed that MLP with a single hidden layer exhibited better performance and shorter training time. Moreover, we determined the optimum number of neurons and the ideal activation function in the hidden layer using the grid search method. For this purpose, we developed various MLPs with varying numbers of hidden neurons and different activation functions, including linear, sigmoid (logistic), binary step, hyperbolic tangent, and Gaussian. The experimental results indicated that MLPs with 24 and 26 hidden neurons provided the best classification performances on the STAFF III and PTBD databases, respectively. Furthermore, the activation function in the hidden and output layers that provided the highest classification performances on both databases was the sigmoid (logistic), which was also the most commonly preferred activation function in the literature for binary classification tasks due to its good generalizability [10, 37, 45, 48]. Consequently, the output of the optimum ANN classifier demonstrates a patient's probability of belonging to one of the two classes (CAD and non-CAD).

The training of the ANN classifier consisted of the feed-forward and back-propagation training parts, which is one of the most commonly used training algorithms for supervised learning [25, 37, 48, 49]. We initially assigned the weights of the ANN classifier arbitrarily using small random and normally distributed numbers. In the course of training, the ANN classifier was exposed to the training set for a predefined number of feed-forward and back-propagation iterations to perform the learning task. During the feed-forward phase, the output of the ANN classifier was calculated for each sample. During the back-propagation phase, the ANN classifier utilized the error in the output to correct its future calculations, aiming to converge towards the desired output. Hence, during back-propagation training, the weights were gradually adjusted to optimize the overall computation carried out by the ANN classifier and minimize the difference between the actual and predicted outputs of the classifier. This difference is commonly referred to as the cost function (E) expressed in Equation 14, where M represents the number of samples in the training set, $\mathbf{o}_i$ denotes the output vector of the ANN classifier, and $\mathbf{d}_i$ corresponds to the target vector for each training pair i.

$$E = \frac{1}{M} \sum_{i=1}^{M} \| \mathbf{d}_i - \mathbf{o}_i \|^2 \tag{14}$$

The back-propagation algorithm is a gradient-descent method used to minimize the mean squared error E, where $\mathbf{w}$ in Equation (16) represents the weight vector between the layers, and η in Equation (15) denotes the learning rate of the ANN classifier, which was optimized as 10^{-3}.

$$\Delta \mathbf{w}_i = -\eta \frac{\partial E}{\partial \mathbf{w}_i}, \qquad 0 < \eta < 1 \tag{15}$$

$$\mathbf{w}_{(i+1)} = \mathbf{w}_i - \eta \frac{\partial E}{\partial \mathbf{w}_i} \tag{16}$$

We periodically evaluated the training length of the ANN classifier using the early stopping regularization method to optimize its performance and prevent over-fitting to the training set due to over-training. Hence, after every predefined number of feed-forward and back-propagation iterations, the current weights were saved, and the performance of the ANN classifier was assessed on the validation set, which represents an estimate of its generalizability on previously unseen data. The training of the ANN classifier was terminated when the mean squared error (MSE) on the validation set was minimized. Thus, by stopping the training early, we avoided the risk of over-optimizing the parameters of the ANN classifier for the training set.

Therefore, we determined the optimum configuration of the ANN classifier with the ideal combination of (hyper)parameters that provides the best classification performance on the independent validation set using the early stopping regularization method. Finally, we evaluated the binary classification performance and generalizability of the optimum ANN classifier on previously unseen data by testing the classifier on the independent test set. We conducted the experiments using a computer equipped with an Intel^R Core^{TM} i7 processor, 16 GB RAM, CPU at 3.60 GHz, and NVIDIA GeForce RTX 2070 GPU. We prepared the software that processes and analyzes the data using MATLAB (R2021) (MathWorks, USA).

Unsupervised clustering technique using Gaussian mixture models and Neyman-Pearson criterion

In order to develop a method that can be used in cases where the abnormal CSNA and ECG data are missing, we propose an unsupervised learning method based on GMM and Neyman-Pearson criterion that performs simultaneous and robust detection of anomalies in the 12-lead normal CSNA and ECG data to realize fast, early, and accurate diagnosis of CADs.

In the literature, GMM has been widely employed as an unsupervised machine learning method for the diagnosis and classification of various CVDs [6, 23, 53, 101–106]. This can be attributed to the numerous advantages of GMM, including its efficiency in clustering and model fitting, its ability to model and estimate a wide range of probability distributions, its capability to effectively handle missing or insufficient data, and its robustness to outliers in the data. Moreover, GMM is a generative method that is capable of generating new synthetic data samples that resemble the original dataset, which can be beneficial for data augmentation tasks. It can also be utilized to identify outliers in the data by assigning low probabilities to data points that do not fit the estimated mixture model, making it very useful in anomaly detection tasks. Furthermore, it provides interpretable parameters for the Gaussian components, which can offer insights into the underlying distribution of the data.

In this study, we performed the optimization of the Gauss parameters ($\mathbf{\Upsilon}$) using the Expectation-Maximization (EM) algorithm to maximize the probability density function (PDF) of the mixture, which is mathematically formulated as a weighted sum of K Gaussian density components, as shown in Equation (18). Here, $\mathbf{x}$ represents the D-dimensional feature vector, π_k denotes the mixture coefficients (weights of the Gaussian components), μ_k corresponds to the mean vector, and $\mathbf{\Sigma}_k$ represents the covariance matrix. The density of each component was mathematically described by the multivariate Gaussian distribution, which is a widely employed statistical model for characterizing data distributions (Equation (17)) [6, 23, 53, 101–106].

$$N(\mathbf{x} \mid \mu_k, \mathbf{\Sigma}_k) = \frac{1}{(2\pi)^{\frac{D}{2}} |\mathbf{\Sigma}_k|^{\frac{1}{2}}} \exp\left\{-\frac{1}{2}(\mathbf{x} - \mu_k)^T \mathbf{\Sigma}_k^{-1}(\mathbf{x} - \mu_k)\right\} \quad (17)$$

$$g(\mathbf{x} \mid \mathbf{\Upsilon}) = \sum_{k=1}^{K} \pi_k \; N(\mathbf{x} \mid \mu_k, \mathbf{\Sigma}_k) \quad (18)$$

The probability density function (PDF) of the Gaussian mixture was parameterized using the Gauss parameters ($\mathbf{\Upsilon}$) in Equation (19), which consists of the mixture coefficients, the mean vector, and the covariance matrix of each component.

The mixture coefficients satisfied the conditions outlined in Equation (20) to assure that the total probability distribution was normalized. This guaranteed that the sum of the mixture coefficients equals one, thereby ensuring that the resulting probability distribution represents a valid PDF.

$$\mathbf{\Upsilon} = (\pi_k, \; \mu_k, \; \mathbf{\Sigma}_k), \qquad k = 1, ., K. \quad (19)$$

$$\sum_{k=1}^{K} \pi_k = 1, \qquad 0 \le \pi_k \le 1 \quad (20)$$

We normalized the 12-lead normal CSNA and ECG features using the min-max normalization method to scale the features of different data types in the same range and to ensure that the developed unsupervised clustering technique assigns equal importance to different data types (i.e., CSNA and ECG data). Hence, by bringing all input variables within a standardized range, our aim was to avoid any bias that may arise due to differences in the scales of the features and to guarantee that the unsupervised clustering technique can accurately learn from the data, thereby assuring fairness in the clustering process.

We independently and randomly divided the whole data in the STAFF III and PTBD databases into non-intersecting training and test sets using the 10-fold cross-validation method to evaluate the performance of the unsupervised clustering technique on previously unseen data, as shown in Tables 9 and 10. Each pattern was used in the test set exactly once in each cross-validation fold to maintain fairness. The test set remained unexposed during the training of the GMM to ensure an unbiased estimate of the technique's performance on previously unseen data.

Table 9: The numbers of the recordings in the training, validation and test sets for the STAFF III database.

Diagnostic Class	Training Set	Validation Set	Test Set	Total
Pre-inflation (Normal)	840	276	132	1,248

The numerical variables are presented as the total number of recordings including all 12-leads.

Table 10: The numbers of the recordings in the training, validation and test sets for the PTBD database.

Diagnostic Class	Training Set	Validation Set	Test Set	Total
Healthy Controls (Normal)	840	276	132	1,248

The numerical variables are presented as the total number of recordings including all 12-leads.

Moreover, we further independently and randomly divided the training sets in the STAFF III and PTBD databases into the training (75 %) and validation (25 %) subsets, as shown in Tables 9 and 10, using the holdout cross-validation method to prevent the GMM from over-fitting to the training sets and ensure better generalization. To assure robust performance evaluation, we averaged the statistical performance results calculated across 10 different cross-validation folds to obtain a single estimation that represents the clustering performance of the optimum GMM for each of the training, validation, and test subsets in the STAFF III and PTBD databases independently.

We estimated the optimum parameters of the Gaussian components ($\mathbf{\Upsilon}$) using the Expectation-Maximization (EM) algorithm, which is an efficient iterative method for finding the maximum likelihood estimation (MLE) of the parameters in statistical models [6, 23, 53, 101–106]. Subsequently, we robustly estimated the joint PDF of the normal CSNA and ECG features by fitting the optimum GMM with the ideal (hyper) parameters, which was optimized to improve the performance of the joint PDF estimation.

Furthermore, we developed a Neyman-Pearson type approach to perform the robust detection of outliers associated with CADs [97, 107]. The Neyman-Pearson decision strategy is based on the concept of statistical hypothesis testing, which includes two competing hypotheses that are the null hypothesis (H_0) and the alternative hypothesis (H_1). It provides an optimal solution to hypothesis testing when making decisions based on limited data while effectively controlling the false-positive and false-negative rates. The objective is to determine which hypothesis is more likely based on the observed data.

We partitioned the 12-lead normal CSNA and ECG features into N equal-length segments, denoted as $X=\{\boldsymbol{x}_1, \ldots, \boldsymbol{x}_N\}$. Each segment was assumed to be independent and identically distributed (i.i.d.), meaning that each segment has the same probability distribution, and all segments are statistically mutually independent. We implemented the Neyman-Pearson decision strategy by calculating the average log-likelihood value of the segments ($P(X \mid H_0)$), as shown in Equation (22), where N represents the total number of segments. Subsequently, we compared these average log-likelihood values with different discrimination thresholds ($\mathbf{\Gamma}$), as shown in the decision rule in Equation (23), where H_1 represents the outliers that correspond to CADs. The decision rule in Equation (23) states that if the average log-likelihood value exceeds the discrimination threshold, the null hypothesis (H_0) was rejected in favor of the alternative hypothesis (H_1).

$$H_0: X \in C_0, \qquad H_1: X \notin C_0 \quad (21)$$

$$P(X \mid H_0) = \frac{1}{N} \log g(X \mid \mathbf{\Upsilon}) = \frac{1}{N} \sum_{i=1}^{N} \log g(\boldsymbol{x}_i \mid \mathbf{\Upsilon}) \quad (22)$$

$$\Theta(X) = \begin{cases} H_0, & P(X \mid H_0) \le \mathbf{\Gamma} \\ H_1, & P(X \mid H_0) > \mathbf{\Gamma} \end{cases} \quad (23)$$

Experimental results and comparative analysis

In this section, we explain and interpret the results of the experiments conducted to evaluate the performance and generalizability of the proposed automated AIHAD technique on the STAFF III and PTBD databases. For this purpose, we computed the confusion matrices to calculate all of the statistical performance evaluation metrics, such as sensitivity (*TPR*) (Eq. (24)), specificity (*TNR*) (Eq. (25)), positive predictive value (*PPV*) (Eq. (26)), negative predictive value (*NPV*) (Eq. (27)), F_1-score (F1) (Eq. (28)), and accuracy (*ACC*) (Eq. (29)). Here, TP, FN, FP, and TN indicate the numbers of the true-positives, false-negatives, false-positives, and true-negatives, respectively.

$$TPR\ (\%) = \frac{TP}{TP + FN} * 100 \tag{24}$$

$$TNR\ (\%) = \frac{TN}{TN + FP} * 100 \tag{25}$$

$$PPV\ (\%) = \frac{TP}{TP + FP} * 100 \tag{26}$$

$$NPV\ (\%) = \frac{TN}{TN + FN} * 100 \tag{27}$$

$$\text{F1}\ (\%) = 2\ \frac{PPV \text{ x } TPR}{PPV + TPR} * 100 \tag{28}$$

$$ACC\ (\%) = \frac{TP + TN}{TP + TN + FP + FN} * 100 \tag{29}$$

The performance results of the automated artificial intelligence based hybrid anomaly detection technique on the STAFF III database

As a result of the implementation of the developed enhanced signal processing technique on the 12-lead wideband raw recordings in the STAFF III database, we simultaneously detected the 12-lead ECG and CSNA signals of all patients. Figures 2 and 3 demonstrate a single lead pre-inflation (normal), inflation (abnormal), and post-inflation CSNA and ECG signals of a patient in the STAFF III database, respectively.

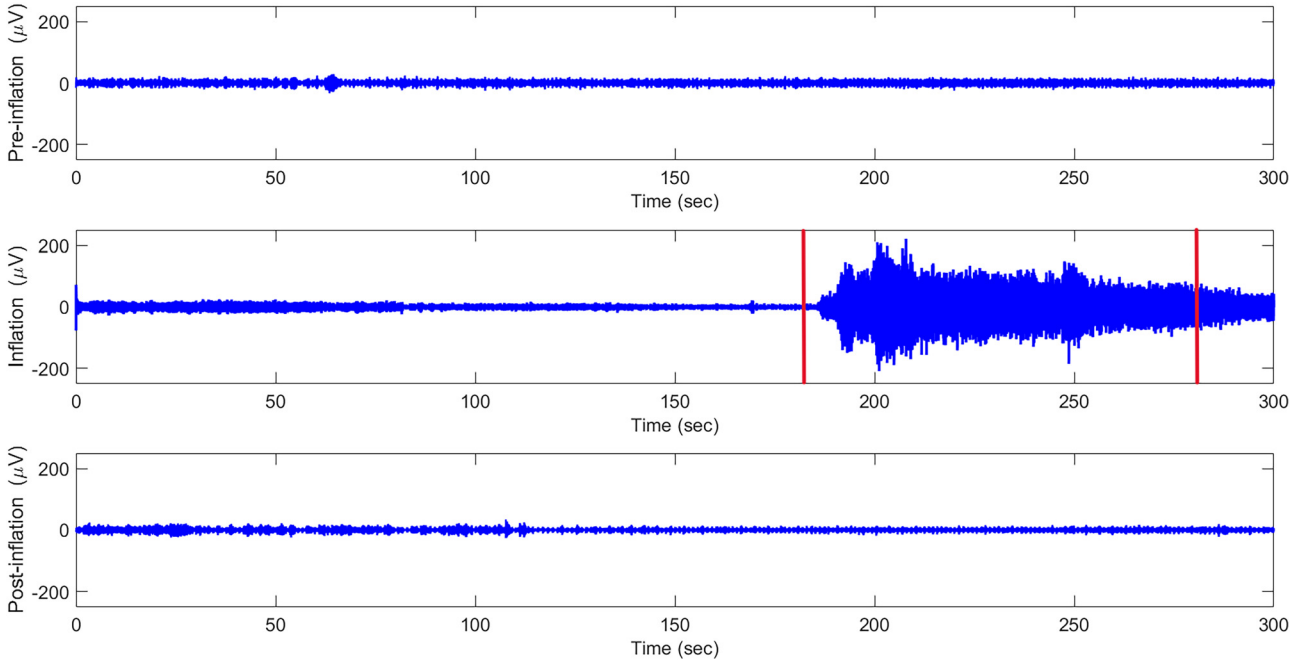

Figure 2: A single lead pre-inflation (normal), inflation (abnormal), and post-inflation CSNA signals of a patient in the STAFF III database that were acquired before, during, and after PCI, respectively. The cardiologists annotated the CBI and CBD times, which are illustrated with red lines at the 182nd second and 280th second, respectively. The inflation (abnormal) CSNA increases shortly after the onset of PCI and decreases after the termination of PCI. Moreover, there is very little difference in the baseline amplitudes of the pre-inflation and post-inflation CSNA signals. This may be due to the fact that these two signals were acquired in different environments with different noise levels, where the former and latter were acquired in the preoperative room and postoperative recovery room of the medical center, respectively.

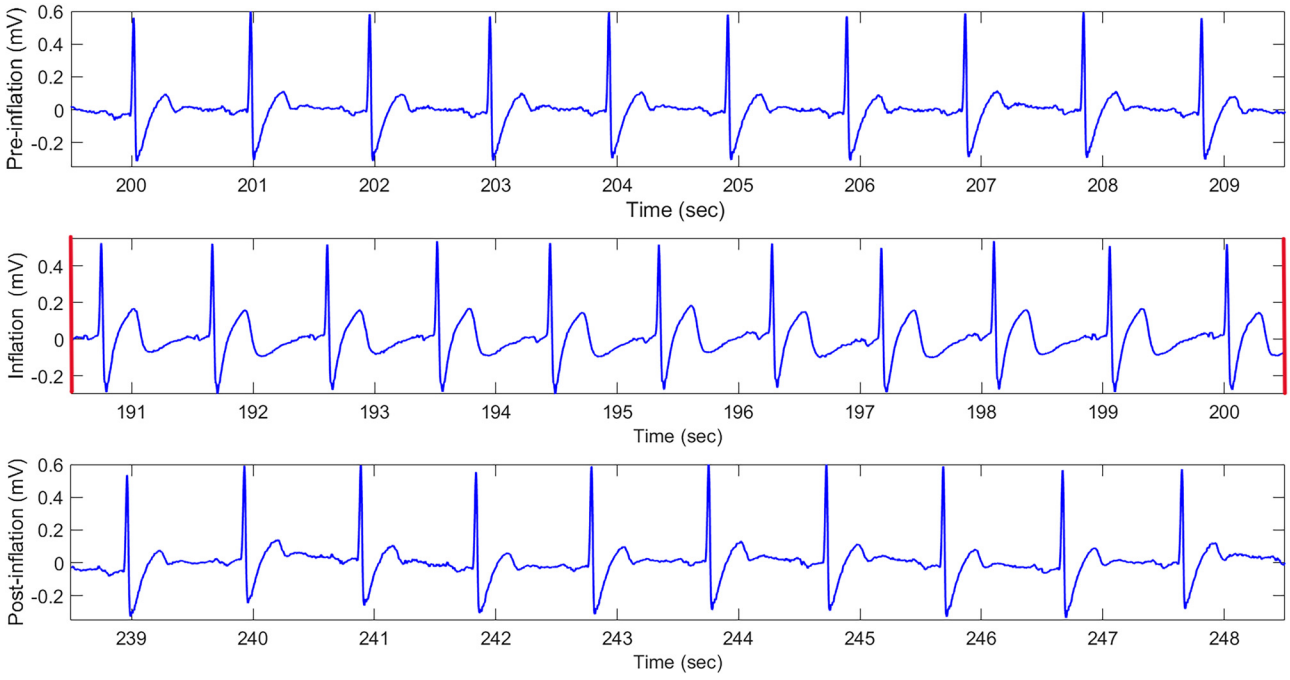

Figure 3: A single lead pre-inflation (normal), inflation (abnormal), and post-inflation ECG signals of the same patient in the STAFF III database that were acquired before, during, and after PCI, respectively. There is an elevation in the ST segment and an increase in the amplitude of the T wave of the inflation (abnormal) ECG signal, which are very common symptoms of ISC. Hence, the anomalies in the ECG signal that occurred during artificially induced ISC were accompanied by the simultaneous increase in the amplitude of CSNA signal.

We considered the pre-inflation (normal) CSNA and ECG signals of each patient as a reference to accurately detect anomalies in the inflation (abnormal) CSNA and ECG signals for the reliable diagnosis of ISC, which is a type of CAD [2–5, 15, 57]. The experimental results on the STAFF III database revealed that there is an increase in the amplitude of the inflation (abnormal) CSNA signals during artificially induced ISC caused by coronary artery occlusion during PCI, which indicates that there is a significant association between CSNA and ISC, as illustrated in Figure 2. This association offers novel perspectives into the relationship between electrical and physiological changes within the cardiac system during ISC, thereby fostering a profound comprehension of the underlying pathological mechanisms [13].

Moreover, the findings of the study demonstrated that the increase in the amplitude of the inflation (abnormal) CSNA signals during artificially induced ISC was accompanied by simultaneous elevation or depression in the ST segment, and polarity or amplitude changes in the T wave of ECG signals, as presented in Figure 3. Therefore, the results suggested that there is a correlation between the increase in the amplitude of CSNA signals and the anomalies in ECG signals during ISC.

Furthermore, the comparison between the inflation (abnormal) and post-inflation signals revealed that the increase in the amplitude of CSNA signals and the anomalies in the ECG signals almost disappeared within several seconds after PCI was terminated (Figures 2 and 3).

Exceptionally, a few patients in the STAFF III database did not demonstrate any anomalies in their inflation (abnormal) CSNA and ECG signals acquired during coronary artery occlusion due to PCI, as depicted in Figure 4. This may be attributed to the relatively shorter duration of PCI or the comparatively small size of the coronary artery in which PCI was performed, which may not have been sufficient to induce ISC in some patients.

For the development of the proposed supervised classification technique, we utilized the 12-lead pre-inflation (normal) and inflation (abnormal) CSNA and ECG data. Moreover, we used only the 12-lead pre-inflation (normal) CSNA and ECG data for the development of the proposed unsupervised clustering technique. The main motivation for developing the unsupervised clustering technique with the Neyman-Pearson criterion that can work using only the pre-inflation (normal) data was to construct a method that can successfully diagnose ISC even in cases where the inflation (abnormal) data are missing.

Table 11 presents the confusion matrix of the hybrid GMM-based clustering technique on the test set of the STAFF III database, which reveals its strong ability to distinguish

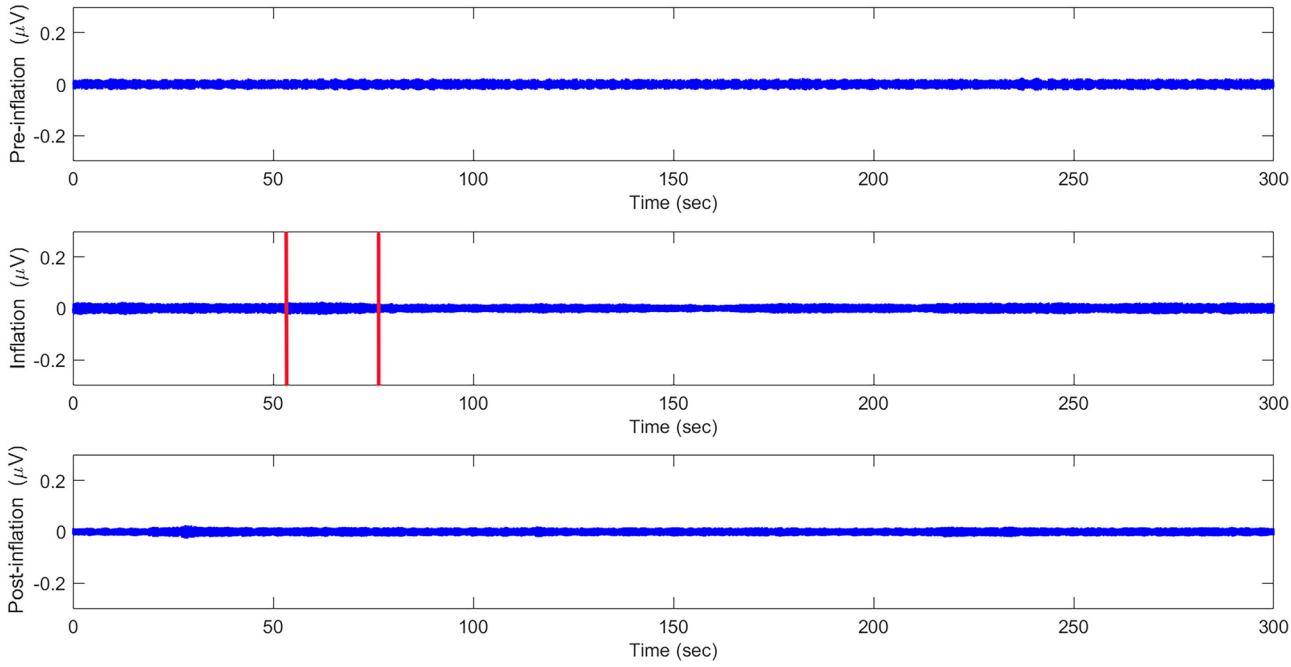

Figure 4: A single lead pre-inflation (normal), inflation (abnormal), and post-inflation CSNA signals of a different patient in the STAFF III database that were acquired before, during, and after PCI, respectively. The cardiologists annotated the CBI and CBD times, which are illustrated with red lines at the 53rd second and 74th second, respectively.

Table 11: The confusion matrix of the hybrid GMM-based clustering technique on the test set of the STAFF III database for CAD diagnosis.

Technique	Confusion Matrix			
			True Label	
			CAD	NON-CAD
GMM_{HYB}	Predicted Label	CAD	True-Positive (TP)=**121**	False-Positive (FP)=**14**
		NON-CAD	False-Negative (FN) = **11**	True-Negative (TN) = **118**

CAD: Coronary Artery Disease; NON-CAD: Not Coronary Artery Disease.

Table 12: The confusion matrix of the hybrid ANN-based classification technique on the test set of the STAFF III database for CAD diagnosis

Technique	Confusion Matrix			
			True Label	
			CAD	NON-CAD
ANN_{HYB}	Predicted Label	CAD	True-Positive (TP)=**127**	False-Positive (FP)=**9**
		NON-CAD	False-Negative (FN)=**5**	True-Negative (TN)=**123**

CAD: Coronary Artery Disease; NON-CAD: Not Coronary Artery Disease.

between patients with and without ISC (i.e., CAD). Out of a total of 132 CAD (abnormal) recordings in the test set, the proposed technique correctly classified 121 recordings, while misclassifying only 11 recordings as non-CAD (normal). Furthermore, out of a total of 132 non-CAD (normal) recordings in the test set, the proposed technique accurately classified 118 recordings, while misclassifying only 14 recordings as CAD (abnormal).

Table 12 shows the confusion matrix of the hybrid ANN-based classification technique on the test set of the STAFF III database, which reveals its strong ability in distinguishing between patients with and without CAD. Out of a total of 132 CAD (abnormal) recordings in the test set, the proposed technique correctly classified 127 recordings, while misclassifying only 5 recordings as non-CAD (normal). Additionally, out of a total of 132 non-CAD (normal) recordings in the test set, the proposed technique accurately classified 123 recordings, while misclassifying only 9 recordings as CAD (abnormal).

Table 13 demonstrates the statistical performance results of the optimum GMM-based clustering technique and the optimum ANN-based classification technique on the test set of the STAFF III database. The performance results of the developed techniques that separately utilized either only 12-lead CSNA data or only 12-lead ECG data are indicated by the notations GMM_{CSNA}, ANN_{CSNA} or GMM_{ECG}, ANN_{ECG},

Table 13: The statistical performance results (%) of the optimum GMM-based clustering technique and optimum ANN-based classification technique on the test set of the STAFF III database for CAD diagnosis.

Performance Measures	12-Lead CSNA Features		12-Lead ECG Features		12-Lead CSNA and ECG Features	
	GMM_{CSNA}	ANN_{CSNA}	GMM_{ECG}	ANN_{ECG}	GMM_{HYB}	ANN_{HYB}
ACC	71.97	77.27	80.30	85.61	**90.53**	**94.70**
TPR	71.21	76.52	81.06	86.36	**91.67**	**96.21**
TNR	72.73	78.03	79.55	84.85	**89.39**	**93.18**
PPV	72.31	77.69	79.85	85.07	**89.63**	**93.38**
NPV	71.64	76.87	80.77	86.15	**91.47**	**96.09**
F1	71.76	77.10	80.45	85.71	**90.64**	**94.78**

The best results are written with bold characters.

respectively. Similarly, the performance results of the hybrid techniques that jointly and simultaneously utilized the 12-lead CSNA and ECG data are represented by the notations GMM_{HYB} and ANN_{HYB}.

The experimental results on the STAFF III database revealed that the proposed ANN-based classification technique has a relatively higher performance for the diagnosis of ISC compared to the GMM-based clustering technique for both separate and joint use of the 12-lead CSNA and ECG data. This can be explained by the fact that the ANN-based classification technique utilizes both the pre-inflation (normal) and inflation (abnormal) data, while the GMM-based clustering technique exclusively utilizes the pre-inflation (normal) data to detect the anomalies in CSNA and/or ECG data.

Moreover, the comparison between the performance results of all developed techniques indicated that the hybrid ANN based classification technique (ANN_{HYB}), which jointly and simultaneously used CSNA and ECG data, achieved significantly higher performance compared to the other techniques that separately used either only CSNA data or only ECG data. Therefore, by taking advantage of the diversity in different data types, the proposed hybrid ANN-based classification technique (ANN_{HYB}) significantly increased the detection performance of ISC. Hence, it can be highly beneficial and useful by providing improved diagnosis, especially for asymptomatic CAD patients with AISC, for whom the diagnostic information provided by ECG alone is not sufficient to reliably diagnose the disease.

Furthermore, the previous studies reported that the sensitivity (TPR) and specificity (TNR) of the gold standard diagnostic test ECG in the diagnosis of ISC were approximately 76 % and 88 %, respectively [2–5, 15, 57]. In this study, the results obtained on the STAFF III database showed that the proposed hybrid ANN-based classification technique (ANN_{HYB}), which jointly and simultaneously uses CSNA and ECG data, exhibits superior sensitivity (TPR) and specificity (TNR) compared to the gold standard diagnostic test ECG in the diagnosis of ISC (Table 13). For these reasons, the hybrid ANN-based classification technique (ANN_{HYB}) was selected as the classification method in the proposed automated AIHAD technique.

Additionally, among the unsupervised machine learning methods developed using only the pre-inflation (normal) data, the hybrid GMM-based clustering technique (GMM_{HYB}), which jointly and simultaneously uses CSNA and ECG data, achieved the best performance. Therefore, it was selected as the clustering method in the proposed automated AIHAD technique.

The performance results of the automated artificial intelligence based hybrid anomaly detection technique on the PTBD database

As a result of the implementation of the developed enhanced signal processing technique on the 12-lead wideband raw recordings in the PTBD database, we simultaneously detected the 12-lead ECG and CSNA signals of all healthy controls and MI patients. Figures 5 and 6 demonstrate a single lead normal and abnormal CSNA and ECG signals of a healthy control and MI patient in the PTBD database, respectively (Figure 4). The experimental results on the PTBD database revealed that there is an increase in the amplitude of the abnormal CSNA signals during MI, which indicates that there is a significant association between CSNA and MI, as illustrated in Figure 5. This association provides novel insights into the relationship between electrical and physiological changes within the cardiac system during MI, thereby facilitating a deeper understanding of the underlying pathological mechanisms [13].

Moreover, the findings of the study indicated that the increase in the amplitude of the abnormal CSNA signals during MI was accompanied by simultaneous elevation or depression in the ST segment, and polarity or amplitude changes in the QRS complex, and the T wave of ECG signals,

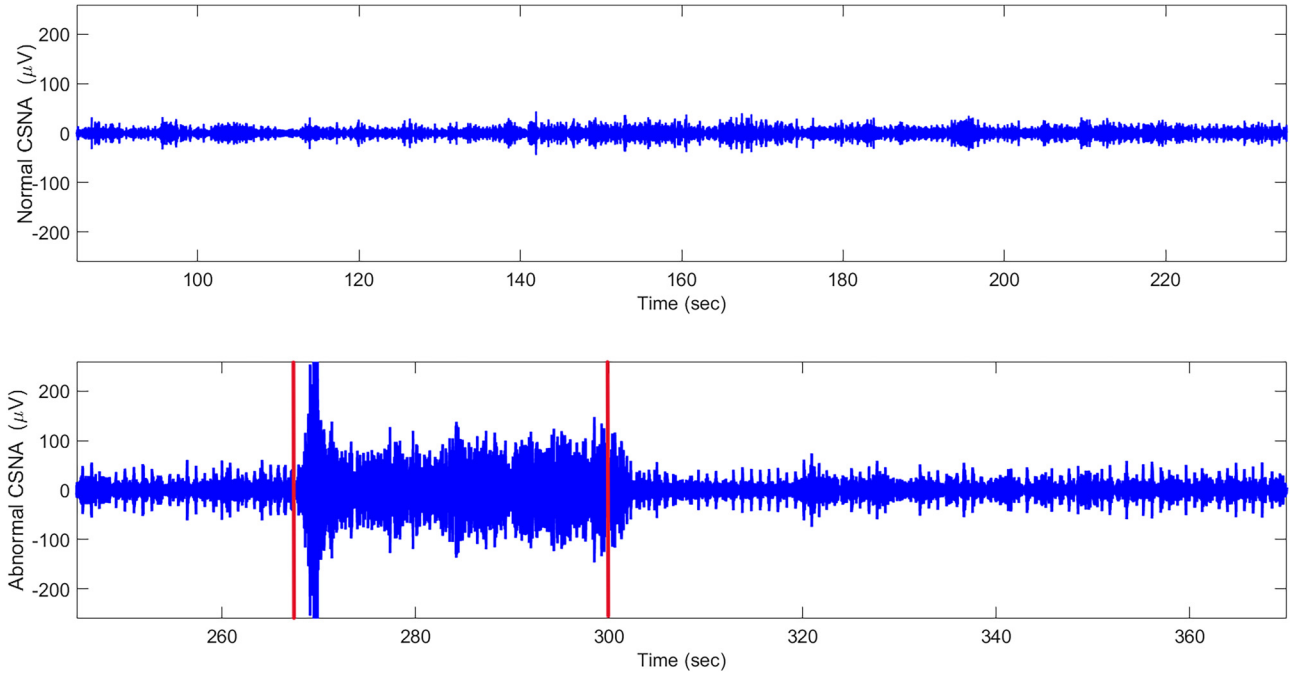

Figure 5: A single lead normal and abnormal CSNA signals of a healthy control and MI patient in the PTBD database, respectively. The cardiologists annotated the onset and end times of MI, which are illustrated with red lines at the 267th second and 300th second, respectively. The abnormal CSNA increases shortly after the onset of MI and decreases after the termination of MI.

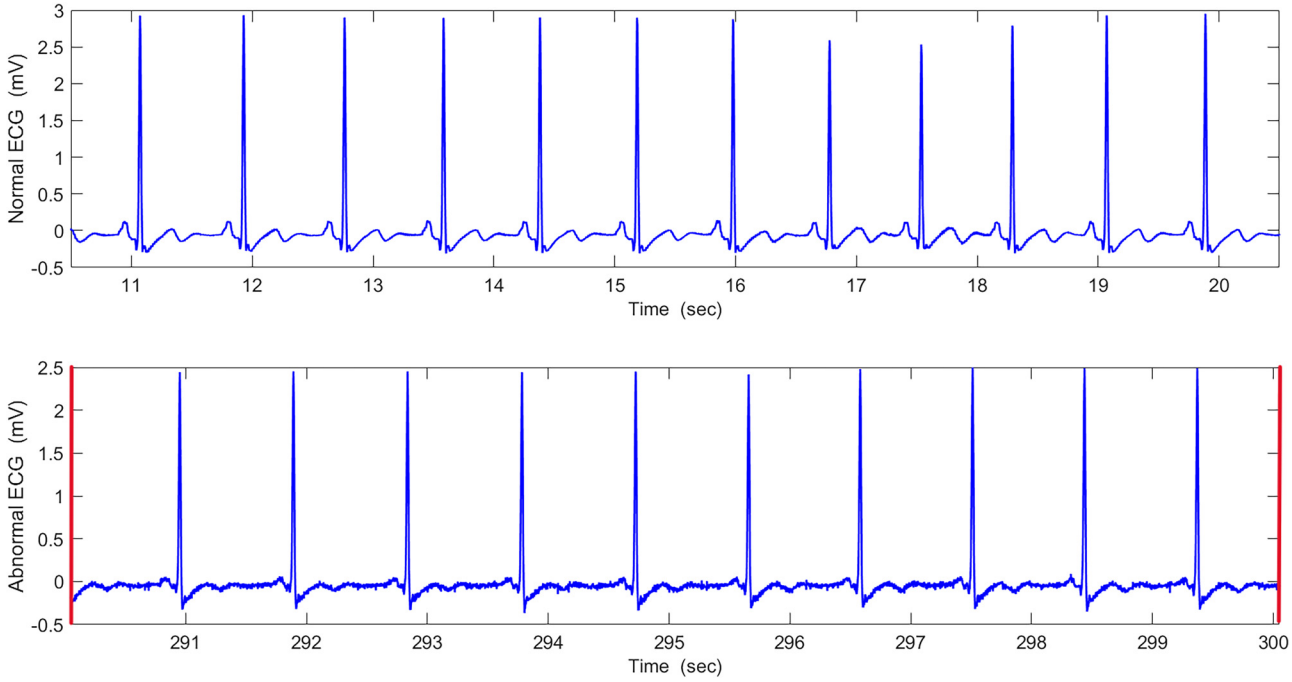

Figure 6: A single lead normal and abnormal ECG signals of the same healthy control and MI patient in the PTBD database, respectively. There is an elevation in the ST segment and a decrease in the amplitude of the QRS complex, and T wave of the abnormal ECG signal, which are very common symptoms of MI. Hence, the anomalies in the ECG signal that occurred during MI were accompanied by the simultaneous increase in the amplitude of the CSNA signal.

as illustrated in Figure 6. Therefore, the results suggested that there is a correlation between the increase in the amplitude of CSNA signals and the anomalies in ECG signals during MI. Thus, the investigations conducted on the STAFF III and PTBD databases showed that CSNA can be utilized as a new biomarker in the diagnosis and classification of ISC and MI, both of which are types of CADs.

For the development of the proposed supervised classification technique, we utilized the 12-lead normal CSNA and ECG data of the healthy controls, and the 12-lead abnormal CSNA and ECG data of the MI patients. Moreover, we utilized only the 12-lead normal CSNA and ECG data of the healthy controls for the development of the proposed unsupervised clustering technique. The main motivation for developing the unsupervised clustering technique with the Neyman-Pearson criterion that can work using only the normal data was to construct a method that can successfully diagnose MI even in cases where the abnormal data are missing.

Table 14 presents the confusion matrix of the hybrid GMM-based clustering technique on the test set of the PTBD database, which reveals its strong ability to discriminate between patients with and without MI (i.e., CAD). Out of a total of 132 CAD (abnormal) recordings of MI patients in the test set, the proposed technique correctly classified 125 recordings, while misclassifying only 7 recordings as non-CAD (normal). Furthermore, out of a total of 132 non-CAD (normal) recordings of the healthy controls in the test set, the proposed technique accurately classified 124 recordings, while misclassifying only 8 recordings as CAD (abnormal).

Table 15 presents the confusion matrix of the hybrid ANN-based classification technique on the test set of the PTBD database, which reveals its strong ability to effectively discriminate between patients with and without CAD. Out of a total of 132 CAD (abnormal) recordings of MI patients in the test set, the proposed technique correctly classified 130 recordings, while misclassifying only 2 recordings as non-CAD (normal). Additionally, out of a total of 132 non-CAD (normal) recordings of the healthy controls in the test set, the proposed technique accurately classified 129 recordings, while misclassifying only 3 recordings as CAD (abnormal).

Table 14: The confusion matrix of the hybrid GMM-based clustering technique on the test set of the PTBD database for CAD diagnosis.

Technique	Confusion Matrix			
			True Label	
			CAD	NON-CAD
GMM_{HYB}	Predicted Label	CAD	True-Positive (TP)=**125**	False-Positive (FP)=**8**
		NON-CAD	False-Negative (FN)=**7**	True-Negative (TN)=**124**

CAD: Coronary Artery Disease; NON-CAD: Not Coronary Artery Disease.

Table 15: The confusion matrix of the hybrid ANN-based classification technique on the test set of the PTBD database for CAD diagnosis.

Technique	Confusion Matrix			
			True Label	
			CAD	NON-CAD
ANN_{HYB}	Predicted Label	CAD	True-Positive (TP)=**130**	False-Positive (FP)=**3**
		NON-CAD	False-Negative (FN)=**2**	True-Negative (TN)=**129**

CAD: Coronary Artery Disease; NON-CAD: Not Coronary Artery Disease.

Table 16 demonstrates the statistical performance results of the optimum GMM-based clustering technique and the optimum ANN-based classification technique on the test set of the PTBD database. The performance results of the developed techniques that separately utilized either only 12-lead CSNA data or only 12-lead ECG data are indicated by the notations GMM_{CSNA}, ANN_{CSNA} or GMM_{ECG}, ANN_{ECG}, respectively. Similarly, the performance results of the hybrid techniques that jointly and simultaneously utilized the 12-lead CSNA and ECG data are represented by the notations GMM_{HYB} and ANN_{HYB}.

The experimental results on the PTBD database revealed that the proposed ANN-based classification technique has a relatively higher performance for the diagnosis of MI compared to the GMM-based clustering technique for both separate and joint use of the 12-lead CSNA and ECG data. This can be explained by the fact that the ANN-based classification technique utilizes both the normal data of the healthy controls and the abnormal data of MI patients to detect the anomalies in CSNA and/or ECG data. On the other hand, the GMM-based clustering technique exclusively utilizes the normal data of the healthy controls to effectively detect the anomalies in CSNA and/or ECG data.

Moreover, the comparison between the performance results of all developed techniques indicated that the hybrid ANN based classification technique (ANN_{HYB}), which jointly and simultaneously used CSNA and ECG data, achieved significantly higher performance compared to the other techniques that separately used either only CSNA data or only ECG data. Therefore, by taking advantage of the diversity in different data types, the proposed hybrid ANN-based classification technique (ANN_{HYB}) significantly increased the detection performance of MI. Thus, the findings of this study indicated that CSNA can serve as an additional diagnostic feature to ECG for considerably increasing

Table 16: The statistical performance results (%) of the optimum GMM-based clustering technique and optimum ANN-based classification technique on the test set of the PTBD database for CAD diagnosis.

Performance Measures	12-Lead CSNA Features		12-Lead ECG Features		12-Lead CSNA and ECG Features	
	GMM_{CSNA}	ANN_{CSNA}	GMM_{ECG}	ANN_{ECG}	GMM_{HYB}	ANN_{HYB}
ACC	76.14	81.44	84.85	89.77	**94.32**	**98.11**
TPR	76.52	81.82	85.61	90.15	**94.70**	**98.48**
TNR	75.76	81.06	84.09	89.39	**93.94**	**97.73**
PPV	75.94	81.20	84.33	89.47	**93.98**	**97.74**
NPV	76.34	81.68	85.38	90.08	**94.66**	**98.47**
F1	76.23	81.51	84.96	89.81	**94.34**	**98.11**

The best results are written with bold characters.

the detection performance of CADs (i.e., MI, ISC, AISC) and decreasing the number of false-negatives, which can lead to reduced mortality and morbidity rates.

Furthermore, the previous studies reported that the sensitivity (*TPR*) and specificity (*TNR*) of the gold standard diagnostic test ECG in the diagnosis of MI were approximately 84 % and 91 %, respectively [1, 9, 28, 53, 81, 83]. In this study, the results obtained on the PTBD database showed that the proposed hybrid ANN-based classification technique (ANN_{HYB}), which jointly and simultaneously uses CSNA and ECG data, exhibits superior sensitivity (*TPR*) and specificity (*TNR*) compared to the gold standard diagnostic test ECG in the diagnosis of MI (Table 16). For these reasons, the hybrid ANN-based classification technique (ANN_{HYB}) was selected as the classification method in the proposed automated AIHAD technique.

Additionally, among the unsupervised machine learning methods developed using only the normal data of healthy controls, the hybrid GMM-based clustering technique (GMM_{HYB}), which jointly and simultaneously uses CSNA and ECG data, achieved the best performance. Therefore, it was selected as the clustering method in the proposed automated AIHAD technique.

Consequently, the results we obtained on the PTBD database using the proposed automated AIHAD technique strongly supported our previous results on the STAFF III database. In addition, the consistently high performance results of the automated AIHAD technique on two different databases that contain different and diverse patients with CADs indicate that the technique is quite robust and generalizable.

Moreover, the performance of the automated AIHAD technique on the PTBD database is relatively higher compared to its performance on the STAFF III database. There are several reasons that may have contributed to this outcome. It is important to consider the characteristics of the two databases to justify the differences in the AIHAD technique's performance on these two databases. Firstly, the ECG patterns obtained during PCI in the STAFF III database may differ from those of patients in the PTBD database who have suffered from MI. Specifically, the anomalies in ECG signals of MI patients in the PTBD database were generally more pronounced, distinct, and apparent compared to those of ISC patients in the STAFF III database [27, 46, 72, 85, 86, 104]. Hence, the data in the STAFF III database are comparatively more difficult to classify than the data in the PTBD database. Secondly, the two databases have different characteristics in terms of the context in which the data was collected. The inflation (abnormal) recordings in the STAFF III database were acquired at the cardiac catheterization laboratory (operation room); however, this was not the case for the PTBD database. Moreover, the recordings in the STAFF III database were acquired during PCI, which implies that they were collected in real-time during an invasive procedure in a clinical setting under specific conditions. Factors such as interference from other medical equipment in the operating room may have introduced noise and artifacts into the raw recordings in the STAFF III database. Therefore, the quality of the raw recordings in the PTBD database may be better than those in the STAFF III database.

Discussion

The accurate and timely diagnosis of CADs is crucial for effective patient treatment and management. The visual and manual interpretation of the 12-lead ECG signals by cardiologists for diagnosing various CVDs is a complex and time-consuming task that requires experienced physicians. Moreover, misdiagnoses are very likely to occur during visual inspection by physicians due to the small amplitudes of ECG signals [9, 12, 19, 27, 32, 44, 48, 70, 79, 104, 108]. Therefore, there is a great need for computer-aided machine learning methods that accurately perform automated

detection of CVDs to reduce the number of misdiagnoses by human experts and decrease the workload of physicians in daily clinical practice.

In patients with CADs, significant anomalies in the ST segment, QRS complex, and T wave of ECG signals occur during ISC and MI [2–6]. However, a considerable number of CAD patients worldwide suffer from AISC, in which there are no anomalies in patients' ECG signals. Hence, ECG alone is limited in its ability to diagnose asymptomatic CAD patients with AISC. Thus, an ECG signal without anomalies does not exclude the possibility of CADs. This limitation makes AISC more dangerous and fatal, as asymptomatic CAD patients with AISC who do not experience any symptoms are prone to misinterpretation by cardiologists, leading to false-negative results.

The significance of this innovative study lies in its proposal of the first automated AI technique that consists of various signal processing, feature extraction, supervised, and unsupervised machine learning methods that jointly and simultaneously analyze 12-lead CSNA and ECG data to perform fast, early, and accurate diagnosis of CADs (i.e., AISC, ISC, MI).

The proposed automated AIHAD technique was implemented on two different publicly available databases to ensure data heterogeneity, and diversify the results and findings of the study. By using the automated AIHAD technique, we demonstrated for the first time that there are anomalies in CSNA signals during CADs, which further supports the well-established fact that there is a direct and strong relationship between the SNS and CVDs [13–15]. Therefore, this study's findings support those of previous studies, which have shown that the SNS plays an important role in regulating the cardiovascular system [13–15].

As discussed earlier, recent studies in the literature have shown a significant association between CSNA and CARs [14, 16]. However, our study is the first to demonstrate a significant association between CSNA and CADs using the proposed automated AIHAD technique, which fills the research gap in the literature. This association offers new perspectives on the connection between electrical and physiological alterations in the cardiac system during CADs, which in turn enhances comprehension of the underlying pathological processes [13].

Moreover, the findings indicated that there is a correlation between the increase in CSNA and the anomalies in ECG signals during CADs. For these reasons, the findings of recent studies [14, 16] and our study collectively suggested that CSNA can be a new biomarker for the diagnosis and classification of both CARs and CADs, respectively.

The performance results of the automated AIHAD technique on the STAFF III and PTBD databases suggested that the technique achieves highly accurate and reliable diagnosis of CADs by simultaneously and robustly detecting anomalies in the 12-lead CSNA and ECG data. Additionally, it has been shown that the automated AIHAD technique achieves superior performance compared to the gold standard diagnostic test ECG in the diagnosis of CADs. This achievement signifies the potential of the automated AIHAD technique to provide an efficient and reliable alternative to the current diagnostic method for diagnosing CADs.

Moreover, the automated AIHAD technique outperformed other AI techniques developed in this study, which separately used either only CSNA data or only ECG data. Therefore, by leveraging the strengths of different data types, the AIHAD technique considerably improved the detection performance of CADs. Hence, the study's findings indicate that CSNA can serve as an additional diagnostic feature to ECG for considerably improving the performance of CAD diagnosis and decreasing the number of false-negatives, potentially leading to reduced mortality and morbidity rates.

The performance comparison between the proposed automated AIHAD technique and previously proposed machine learning approaches that used only ECG data to diagnose or classify CADs is summarized in Table 17, which presents all statistical performance evaluation metrics to comprehensively evaluate the effectiveness of the AIHAD technique.

Magrans et al. aimed to develop a non-linear SVM model with a radial basis function (RBF) kernel to detect CAD [57]. The feature selection was done using a univariate statistical test and an algorithm for sequentially selecting the most important statistically significant variables. The grid search method was used to optimize SVM parameters and generate the final prediction model. Repeated 5-fold cross-validation was used to estimate the generalization performance. The model had a sensitivity of 83.3 %, specificity of 91.7 %, precision of 90.9 %, and negative predictive value (*NPV*) of 85.7 %.

Sadhukhan et al. proposed using the harmonic phase distribution pattern of ECG data for MI identification [44]. The morphological and temporal changes of the ECG waveform caused by the presence of MI were reflected in the phase distribution pattern of the Fourier harmonics. The changes in the ECG waveform morphology were clearly manifested as changes in the relative phases of the harmonic components. Two discriminative features that reflect these variations were identified for 3-lead ECG. The binary classification was performed using a threshold-based classification rule and logistic regression. The model achieved an accuracy of 95.6 %, sensitivity of 96.5 %, and specificity of 92.7 %. The algorithm was then implemented and validated

Table 17: The performance comparison between the proposed automated AIHAD technique and recent machine learning studies that used only ECG data for CAD diagnosis or classification.

Study	Technique	Database	TPR (%)	TNR (%)	PPV (%)	F1 (%)	ACC (%)	NPV (%)
Magrans et al. [57]	SVM	STAFF III database	83.3	91.7	90.9	–	–	85.7
Proposed method	**AIHAD**	**STAFF III database**	**96.21**	**93.18**	**93.38**	**94.78**	**94.70**	**96.09**
Sadhukhan et al. [44]	Logistic regression	PTBD database	96.5	92.7	–	–	95.6	–
Tripathy et al. [41]	LS-SVM	PTBD database	99.8	99.6	–	–	99.7	–
Dohare et al. [8]	SVM	PTBD database	96.6	96.6	–	–	96.6	–
Ahmad et al. [56]	SVM	PTBD database	94	–	98	–	98.4	–
Acharya et al. [29]	KNN	PTBD database	99.4	96.2	–	–	98.8	–
Sharma et al. [28]	KNN	PTBD database	98.3	99.4	99.4	–	99	–
Jothiramalingam et al. [51]	KNN	PTBD database	77.4	81.8	–	–	82.8	–
Sraitih et al. [59]	Random forest	PTBD database	73	–	74	–	75	–
Agrawal et al. [49]	Decision tree	PTBD database	–	96.5	–	–	98.3	–
Liu et al. [109]	Random tree	PTBD database	94.2	74	–	–	89.5	–
Chang et al. [53]	GMM	PTBD database	85.7	79.8	–	–	82.5	–
Proposed method	**AIHAD**	**PTBD database**	**98.48**	**97.73**	**97.74**	**98.11**	**98.11**	**98.47**
Al-Zaiti et al. [11]	GBM	Self-collected ECG data	77	76	43	–	–	94
Daraei et al. [61]	J48 (C4.5)	Self-collected ECG data	86.6	–	–	80	82.6	–
Sun et al. [4]	SVM, BT	Self-collected ECG data	91.7	82.7	–	–	89.1	–
Bashir et al. [60]	Naive Bayes, SVM, Decision tree	UCI machine learning repository	93.7	92.8	–	82.1	87.3	–
Ramasamy et al. [39]	KNN	MIT-BIH database	95.4	99.4	–	–	99.4	–
Exarchos et al. [67]	Association rule mining	European ST-T database	87	93	–	–	–	–

on a commercially available microcontroller based Arduino board. The firmware used the pretrained logistic regression classifier. The model did not outperform all earlier reported techniques, but it has computational simplicity of the features, reduced feature dimension, and use of simple linear classifiers. The drawback of this study is the use of only 3-lead ECG, which can limit the detection performance of certain types of MI.

Tripathy et al. proposed an approach for the detection of MI using multi-resolution analysis of 12-lead ECG signals [41]. Baseline wander noise in ECG data was filtered out using a high-pass filter. The filtered ECG data was segmented using a rectangular window. The segmented ECG frames were subjected to FBSE-based empirical wavelet transform (FBSE-EWT) for the time-scale decomposition of the 12-lead ECG signals. For each ECG lead, nine subband signals were evaluated using FBSE-EWT to extract the statistical features. The deep layer least-squares SVM (DL-LSSVM) classification layer, which was formulated using the hidden layers of sparse auto-encoders and the LSSVM, was used for the detection of MI from the feature vector of 12-lead ECG. The entropy features were shown to be more significant for the detection of MI and exhibited higher performance using the proposed classifier compared to the kurtosis and skewness features, which failed to capture the pathological variations in the subband signals. The combination of FBSE-EWT-based entropy features and DL-LSSVM had an accuracy of 99.7 %, sensitivity of 99.8 %, and specificity of 99.6 %.

Dohare et al. proposed a method for detecting CAD using 12-lead ECG data and analyzed each lead with the help of a composite lead [8]. The min-max normalization method was used to rescale the attributes. The raw signal was preprocessed by a two stage median filter to remove baseline drift using a sliding window. The composite lead was used to detect ECG wave components and clinical wave intervals. The complexes of the composite signal were enhanced using the sixth power of the signal. The mean value of the enhanced signal was used as the threshold to determine the high peak of the QRS of the composite signal and individual leads at a variable window size. The four clinical ECG features were determined globally from the average beats of the 12-lead ECGs. Peak-to-peak amplitude, area, mean, standard deviation, skewness, and kurtosis were determined for the ECG features. The binary classification for the detection of CAD was performed using a simple SVM classifier with an RBF kernel. After implementing principal component analysis (PCA) as a feature dimension reduction method to reduce the number of features and computational complexity, the sensitivity remained the same (96.6 %), while the specificity (96.6 %), and accuracy (96.6 %) were slightly reduced.

Ahmad et al. proposed two computationally efficient multimodal fusion frameworks for MI detection, called

Multimodal Image Fusion (MIF) and Multimodal Feature Fusion (MFF) [56]. At the input of these frameworks, they converted the raw ECG data into three types of two-dimensional (2D) images using three different statistical methods, which are Gramian Angular Field (GAF), Recurrence Plot (RP), and Markov Transition Field (MTF). In MIF, they performed image fusion by combining three grayscale input images (GAF, RP, MTF) to create a three-channel colored single image that served as input to the CNN. They used AlexNet CNN and the softmax classifier for feature extraction and classification tasks, respectively. The limitation of the MIF framework was that it required exactly three different statistical grayscale images to create a three-channel compound image. In MFF, they transformed ECG heartbeats into GAF, RP, and MTF images. They extracted the features from the penultimate layer of AlexNet CNN, which consisted of three convolutional layers, two pooling layers, and one fully connected layer. By using a Gated Fusion Network (GFN), they fused these extracted features, which were finally used to train an SVM classifier. MFF yielded higher performance compared to MIF. The limitation of the MFF framework was that it required using three separate AlexNet CNNs for training on the GAF, RP, and MTF images, which necessitated more time for training and inference. The SVM classifier performed better than the softmax classifier. They achieved a classification accuracy of 98.4 %, sensitivity of 94 %, and precision of 98 %. They concluded that the multimodal fusion of the modalities increased the performance of the machine learning task compared to using the modalities individually. The disadvantage of this study is the use of only one-lead ECG, which can limit the detection performance of certain types of MI.

Acharya et al. introduced a method for the automated detection and localization of MI [29]. Firstly, ECG signals were pre-processed to eliminate noise and baseline wander using a wavelet basis function. Using the Pan–Tompkins algorithm, the pre-processed ECG signals were segmented and subjected to discrete wavelet transform (DWT) up to four levels of decomposition. Thus, a total of eight DWT coefficients were obtained and twelve nonlinear features were extracted from these coefficients. Feature ranking methods, such as Student's t-test and ANOVA, were used to rank the extracted features according to their significance. The selected significant features were used for binary and multiclass classification using a KNN classifier for the detection and localization of MI, respectively. The ranked features were fed into the KNN classifier one by one to find the minimum number of features necessary for obtaining the highest classification performance. The classifier exhibited an average accuracy of 98.8 %, sensitivity of 99.4 %, and specificity of 96.2 % for MI detection. They claimed that the method can be used as an automated diagnostic tool for the detection of MI using 12-lead ECG and the localization of MI using one-lead ECG.

Sharma et al. presented a technique for the detection and localization of MI using one-lead ECG [28]. Firstly, the ECG signals were segmented into short-duration ECG segments, which were then passed through a two-stage median filter to remove baseline wander. This was followed by a Savitzky-Golay filter to obtain smoothened ECG segments, which were decomposed into wavelet bands using stationary wavelet transform (SWT), so that they can be analyzed at different frequencies. Energy, entropy, and slope-based features were extracted at specific wavelet bands from the decomposed ECG segments. The relevance of the features was measured on the basis of Fisher score. The top-ranked features were fed to the KNN classifier with Mahalanobis and Euclidean distance functions to perform binary classification for MI detection. To handle the imbalanced data, the adaptive synthetic (ADASYN) sampling approach was employed due to disparity in the instance space. They utilized 10-fold cross-validation for both MI detection and localization. The technique has shown a sensitivity of 98.3 %, specificity of 99.4 %, precision of 99.4 % and accuracy of 99 % for MI detection using top-ranked features. The drawback of this study is the use of only one-lead ECG, which can limit the detection and localization performance for certain types of MI.

Jothiramalingam et al. proposed a polynomial curve-fitting technique based on optimization strategies to diagnose CAD [51]. Firstly, the noises in ECG signals were removed using a DWT. The ECG signals were then partitioned using a Hamming window. The polynomial coefficients were obtained by choosing the best polynomial order using the genetic algorithm (GA) and particle swarm optimization (PSO) algorithm. Using these polynomial coefficients, five features were computed, including area, variance, kurtosis, root mean, and form factor. These features were fed into different classifiers to perform binary classification, such as MLP, SVM, KNN, Levenberg–Marquardt Neural Network (LMNN), and Scaled Conjugate Gradient Backpropagation Neural Network (SCGBNN). The GA and PSO-based classifiers achieved good performances compared to classifiers that were not based on GA and PSO. The highest classification performance was achieved using the KNN classifier, with a sensitivity of 77.4 %, specificity of 81.8 %, and accuracy of 82.8 %.

Sraitih et al. investigated an automatic CAD detection system using ECG data and presented an approach to evaluate its robustness in classifying CAD under different types of noise [59]. The preprocessing stage consisted of normalizing 12-lead ECG signals using the min–max normalization

method. They used a low-pass Butterworth filter to remove the noises from the ECG data. They employed three well-known supervised machine learning models, which are SVM, KNN, and random forest, and tested their performances in classifying normal and CAD classes. These models were trained on the preprocessed data and no feature extraction was performed. They conducted a grid search on each model by supplying a mixture of parameter grids to obtain the appropriate combinations of hyper-parameters that provide the most accurate predictions. The performances of all the models in detecting CAD were low, especially in detecting the normal class samples. Random forest obtained the best performance in predicting CAD with an accuracy of 75 %, precision of 74 %, and sensitivity of 73 %. While dealing with the noisy test set, the SVM classifier outperformed the other models with an accuracy of 68 %, precision of 66 %, and sensitivity of 66 %.

Agrawal et al. investigated the application of machine learning techniques on the vector magnitude data of heart signals generated via Vectorcardiography (VCG) to distinguish CAD patients from healthy subjects [49]. To eliminate low-frequency noise in cardiac signals, the patients' VCG data were filtered using a bandpass filter via Biopac Acqknowledge software's built-in functions. Vector magnitude was derived from patients' orthogonal VCG leads using the 3D Pythagorean theorem. Each patient's QT and RR intervals were marked on the vector magnitude using Biopac Acqknowledge software's computer-assisted manual marking methods. The statistical features were extracted from the QT and RR intervals and used as inputs for machine learning techniques, such as ANN, SVM with RBF kernel, and decision tree, to perform binary classification. Stratified 10-fold cross-validation was employed for all models. Results indicated that vector magnitude-derived QT variability has more predictive value than RR variability in classifying CAD patients, and it showed a higher contribution towards increased accuracy of the prediction class. However, adding the RR variability to obtain combined variables further improved the overall performance. Decision tree generated relatively higher performance for CAD classification with an accuracy of 98.3 % and specificity of 96.5 %, while using fewer predictor variables than other models. IBM SPSS Modeler and KNIME were employed as the software platforms.

Liu et al. proposed an ECG feature for CAD detection by fitting a given ECG signal with a 20th-order polynomial function, which they defined as PolyECG-S [109]. First, a DWT was employed to remove high-frequency noise and baseline shifting from ECG signals. Next, all the R peaks in the ECG signals were detected using the wavelet transform and all the ECG signals were split into ECG cycles, which were normalized on both the time and voltage axes to make different ECG signals comparable to each other. The polynomial function was fitted to the ECG signals, and each ECG cycle was represented as a vector of the coefficients of this polynomial function. Akaike information criterion (AIC) was used to determine the best choice of the polynomial fitting function order with the minimum AIC value. The optimal similarity between the PolyECG-S curve and ECG signals was observed when the polynomial fitting function order was 20. The fitted coefficients were defined to be the ECG representing features. The best feature subsets were chosen by the feature selection algorithms, such as GA and PSO. There were seventeen features chosen by GA and seven features chosen by PSO, respectively. The two feature subsets chosen by GA and PSO were tested for their discrimination performance with four classification models, which are J48 decision tree, random tree, SVM, and naive Bayes. The feature selection and binary classification models were formed using the Weka software, and the software's default parameters were utilized. The top CAD detection model was the J48 decision tree with the feature subset chosen by GA, which showed an accuracy of 89.5 %, sensitivity of 94.2 %, and specificity of 74 %. The disadvantage of this study is that although different individuals have different optimal polynomial fitting functions for their ECG signals, the polynomial fitting function's order was set to be the same for all individuals.

Chang et al. presented a diagnosis system for classifying CAD by converting 4-lead ECG data into a density model [53]. During ECG signal segmentation, the location of the R peak was used to divide the ECG complex into separate heartbeats. A hybrid system combining HMM and GMM was used to classify 4-lead ECG data. Four HMMs were used to learn the 4-lead ECG complex and to calculate the probability of the state change in each lead. These probabilities were further converted into the log-likelihood values, which were treated as different statistical feature vectors that were then given as input to GMM and SVM. The 16-State HMMs were trained using CAD data, so that CAD and normal data can have differences in likelihood values. The four-dimensional (4D) feature vector extracted by the four HMMs was clustered by GMM with different numbers of distributions. The density model of data distribution was fitted by the maximum likelihood estimation (MLE) using the expectation–maximization (EM) algorithm via the NETLAB tool. The SVM classifier with the RBF kernel function was also utilized for binary classification, since the data were linearly inseparable. The combination of HMMs as a feature extraction tool and GMM as a classification tool performed much better for CAD detection when the data distribution was overlapped, as the feature space in this study. The

sensitivity, specificity, and accuracy were 85.7 %, 79.8 %, and 82.5 %, respectively. They claimed that this was because the 4D feature inputs were very challenging to classify. The disadvantage of this study is that the length of each heartbeat was fixed to 400 points.

Green et al. employed ANN ensembles on ECG data to detect acute coronary syndrome (ACS), which is a type of CAD [45]. The ECG data were acquired from ACS patients presenting to an emergency department with chest pain. Feature reduction was accomplished using PCA and 16 PCA variables were used for the training of the models. The cross-entropy error function was used, which was minimized using the gradient descent method. Two methods were used for constructing the ensemble models, which were the bagging method and S-fold cross-splitting. Bagging ensemble contained MLPs trained on bootstrap samples of the original training set. Model selection was performed using a grid search and the best model was found to be an ANN cross-splitting ensemble trained on only the ECG data. Hence, they found an advantage in using ANN ensembles compared to both MLPs and logistic regression. The addition of clinical data did not improve the performance of the ANN ensemble. At the sensitivity of 95 %, the specificity was 41 %, corresponding to an NPV of 97 %. They claimed that the ensemble model, combined with the judgment of trained emergency department personnel, could be useful for the early discharge of chest pain patients. The limitation of the study is the relatively small study population.

Al-Zaiti et al. used ANN, logistic regression, and gradient boosting machine (GBM) for the prediction of ISC in patients with chest pain using only the 12-lead ECG [11]. First, they preprocessed all ECGs using manufacturer-specific commercial software and manually inspected tracings for noise and artifacts. After ectopic beats were removed and median beats were computed, they extracted the temporal–spatial ECG features from each prehospital ECG using previously validated commercial algorithms. Feature selection and annotation based on existing clinical knowledge boosted the classification performance of linear prediction models like logistic regression. This is reasonable given that data reduction and labeling could reduce the dimensionality and complexity in the data. Nonlinear models like ANN and GBM were more powerful tools to handle the high-dimensional and highly correlated nature of ECG features. They trained and tested the performance of these three classifiers on two independent prospective patient cohorts using the same temporal-spatial features. They employed the classifiers with the best low bias–low variance trade-off to create a simple machine learning fusion classifier, which showed a sensitivity of 77 %, specificity of 76 %, precision of 43 %, and NPV of 94 %. Supplementing the algorithm with patient history data did not improve classification performance. They claimed that the model can be used as a clinical decision support tool, when combined with the judgment of trained emergency department personnel, to help improve clinical outcomes in patients with chest pain.

Daraei et al. presented a prediction model for MI using classification data mining methods that consider the imbalanced nature of the problem [61]. Firstly, the min-max normalization method was applied to scale the features' values. A hybrid feature selection method, including GA and Weight by Relief, was then applied to select the best subset of features. Top-weighted features selected by the Weight by Relief method were given to GA for choosing the best final features. Feature selection improved the performance of both cost-sensitive and cost-insensitive models. Metacost classifier was applied to create a cost-sensitive J48 (C4.5) decision tree by assigning different cost ratios for misclassified cases. Implementing the cost-sensitive J48 decision tree on the imbalanced dataset provided better results compared to not using a cost-sensitive model. Moreover, making J48 decision tree cost-sensitive improved performance over traditional classifiers. Using the hybrid feature selection method along with cost-sensitive classification method yielded an accuracy of 82.6 %, sensitivity of 86.6 %, and F-measure of 80 %, respectively. Rapidminer was used to implement the proposed model. The limitation of the study is the unavailability of the Q-wave features and rhythm in the dataset.

Sun et al. presented a method for the detection of ISC in patients with subtle ECG waveform changes using ensemble learning to integrate ECG dynamic features obtained via deterministic learning [4]. Wavelet transform-based analysis was performed to remove the noise in the 12-lead ECG signals, which were then linearly converted to 3-lead VCG signals using the Kors matrix to minimize computational complexity. The dynamic modeling of VCG by deterministic learning was implemented to generate a cardiodynamicsgram. Three low-dimensional and discriminative dynamic features, namely spectrum fitting exponent, Lyapunov exponent, and Lempel-Ziv complexity, were extracted from the cardiodynamicsgram. Random feature selection was used to obtain different feature subsets. A random sampling method was employed to generate various data subsets for each feature subset to train multiple individual classifiers, including SVM with an RBF kernel, SVM with a linear kernel, and a boosting tree. Subsequently, the bagging-based heterogeneous ensemble learning algorithm was applied to these features to generate different base classifiers. The bagging algorithm was used to fuse outputs of different individual base classifiers using a weighted voting method to generate a final classifier for ISC detection. The

heterogeneous ensemble learning algorithm exhibited an accuracy of 89.1 %, sensitivity of 91.7 %, and specificity of 82.7 % using repeated 5-fold cross-validation. They claimed that the proposed ensemble model that fused SVM and the boosting tree outperformed conventional base classifiers and homogeneous ensemble models. However, their proposed ensemble model did not achieve better results on the external test set, which was obtained from a different medical center.

Bashir et al. proposed a weighted vote-based ensemble model for the prediction of CVDs [60]. Firstly, different preprocessing techniques were used to clean the data. They claimed that the proposed ensemble model overcomes the limitations of conventional data-mining techniques by combining different types of heterogeneous classifiers, including SVM, naive Bayes, decision tree, and instance-based learner. They used a weighted vote-based ensemble technique to combine all the trained individual classifiers. They employed the 10-fold cross-validation method to alleviate the insufficiency of samples. The ensemble model exhibited an accuracy of 87.3 %, sensitivity of 93.7 %, specificity of 92.8 %, and F-measure of 82.1 %. It achieved higher performance compared to the other individual classification techniques. RapidMiner was used for model building, training, and testing.

Ramasamy et al. presented a rhythm-based approach to screen patients with CARs at the primary level [39]. During pre-processing, various noises associated with the ECG signals were removed. The R peaks in the ECG signals were located, and the signals were segmented based on the R peak locations to detect a single heartbeat. The FBSE features of the segmented ECG signals were extracted by computing the Fourier-Bessel coefficients using the FBSE method on the segmented ECG beats. The feature vector dimensions were reduced using PCA to acquire low-dimensional FBSE features for reducing the computational complexity. These features were used as input to the Jaya-optimized ensemble random subspace KNN (JO-ERSKNN) classifier to classify five types of CAR beats. Jaya optimization was applied to gradually tune the hyper-parameters of the ensemble random subspace KNN classifier. The model demonstrated an accuracy of 99.4 %, sensitivity of 95.4 %, and specificity of 99.4 % for classification of CARs. They claimed that the model can be made compatible with various wearable devices.

Exarchos et al. presented an automated methodology based on association rules for the detection of ISC in long-duration ECG recordings [67]. During preprocessing, the noise was removed from the ECG signals. The ECG features were extracted from the ST segment and T wave of ECG beats. The features were then discretized by transforming the continuous-valued features into categorical using the modified classification tree algorithm. This tree was created from the training set during the discretization stage and was applied to classify the cases in the test set. They used an association rule extraction algorithm and a rule-based classification model to perform binary classification. The classification tree discretizer combined with predictive association rules algorithm yielded higher classification performance and required less time for rule generation. The model showed a sensitivity and specificity of 87 and 93 %, respectively. They claimed that the model has the ability to provide interpretation for the decisions made, due to the employment of association rules for classification. The disadvantage of the study is that the association rules method can also find spurious relationships among the data.

The performance of the proposed automated AIHAD technique is superior to that of most previously proposed machine learning approaches that exclusively used ECG data to diagnose or classify CADs. Specifically, the binary classification performance results of the automated AIHAD technique on the PTBD database demonstrated higher sensitivity (TPR), higher specificity (TNR), higher accuracy (ACC), comparable precision (PPV), and higher negative predictive value (NPV) compared to most of the existing studies in the literature that utilized machine learning methods and only ECG data to diagnose or classify CADs (Table 17).

Moreover, the performance comparison between the proposed automated AIHAD technique and previously proposed deep learning approaches that used only ECG data to diagnose or classify CADs are summarized in Table 18. Most of the existing deep learning methods are based on the development of various CNN architectures commonly trained using transfer learning or fine-tuning methods and using only ECG data to diagnose or classify various CVDs [3, 12, 69, 71, 72, 74].

Brisk et al. conducted a retrospective and observational study designed to assess the feasibility of detecting induced CAD in human subjects earlier than experienced cardiologists using a deep CNN trained with transfer learning [73]. Firstly, ECG signals were split into short-length ECG segments. They used a 34-layer CNN that had residual connections culminating in a fully connected layer with a single and sigmoid-activated output node. The model was evaluated using the 10-fold cross-validation and the loss was calculated using binary cross-entropy. The model achieved a sensitivity of 84.2 %, specificity of 94.7 %, accuracy of 80.3 %, and F1-score of 81.4 %. They claimed that the dataset was too small for the model to achieve meaningful performance, despite the use of transfer learning. The study highlighted the risk of deep learning models leveraging data leaks to produce spurious and falsely high results. The drawback of

this study is that the model was initiated using weights from the CAR detection task, on the assumption that the ECG features learned during CAR detection would improve the generalization for CAD detection, which may not be accurate for all types of CADs.

Reasat et al. presented a shallow CNN architecture for the detection of MI using 3-lead ECG signals [71]. Firstly, each signal was downsampled from 1 kHz to 250 Hz. A two-stage median filter was then used to remove baseline wander. Next, Savitzky-Golay smoothing filter was used to remove other noises. The denoised signal was further downsampled to 64 Hz to decrease computational burden and speed up training time. The signals were then partitioned into short-length ECG segments. The CNN benefited from the use of varying filter sizes in the same convolutional layer, which allowed it to learn features from signal regions of varying length. Feature maps extracted by the inception blocks were concatenated and passed on to a global average pooling layer. Lastly, there was a two-unit dense layer with a softmax activation layer, which gave the categorical probability. The weights of the dense layer were L2 regularized to prevent over-fitting. The back-propagation training algorithm and the Adam optimizer was used to update the weights. A subject-oriented approach was used, in which the CNN was tested on one patient and trained on the rest of the patients. The model achieved an accuracy of 84.5 %, sensitivity of 85.3 %, and specificity of 84.1 % when compared to the benchmark. The model was implemented using the Keras neural network library.

Makimoto et al. presented a CNN equipped with a 6-layer architecture to diagnose MI using ECG images obtained from a reduced and optimized number of ECG leads [74]. During the network training, they incorporated data augmentation to increase the learning efficacy. They generated activation maps of the final convolutional layer using Grad-CAM to visualize the CNN's focus points on the ECGs during its MI recognition. They observed that the CNN focused strongly on the ST segment and T wave elevation in the ECG to diagnose MI, as cardiologists do. The model was then tested together with 10 physicians using the data in the test set and their MI recognition performances were compared. The performance of the CNN model was higher compared to those of the physicians. The method revealed an accuracy of 75 %, sensitivity of 65 %, specificity of 86 %, precision of 82 %, NPV of 71 %, and F1-score of 72 %. Hence, they suggested that a simple 6-layer CNN architecture derived from a small ECG database may achieve comparable capability compared to cardiologists in recognizing MI using ECG images. Additionally, ECG image compression up to a quarter resolution did not significantly decrease the MI detection capability of the CNN.

Hammad et al. presented a method based on an end-to-end deep CNN model to perform binary classification for automated detection of MI using ECG data [75]. The proposed CNN model included three blocks of 1D convolutional layers, batch normalization, dropout operation, two dense layers, rectified linear unit (ReLU), and softmax activation functions. To reduce the impact of imbalanced ECG data, they focused on the loss of the minority classes and optimized the model using the focal loss function. They used the Adam optimization algorithm and stratified 5-fold cross-validation. The proposed method using the focal loss performed better and converged earlier than the one without using the focal loss. It showed an overall accuracy of 89.7 %, precision of 88.5 %, sensitivity of 81.1 %, and F1-score of 83 %.

Darmawahyuni et al. suggested sequence modeling based on a long short-term memory (LSTM) network for the binary classification of sequential ECG data to automatically detect MI using ECG signals [82]. The performance of the proposed method was compared to that of the standard RNN and gated recurrent unit (GRU). The best sequence model classifier was found to be LSTM with a 90 %:10 % training and test set split. They claimed that a simple LSTM network presented better performance results in the training and test sets compared to the standard RNN and GRU architectures with identical hyper-parameters. Specifically, LSTM had a sensitivity of 98.4 %, specificity of 97.9 %, precision of 95.6 %, and F1-score of 96.3 %, respectively. They stated that LSTM was able to learn and select which data needs to be stored or discarded, which resulted in its better performance compared to the standard RNN and GRU.

Feng et al. used a combined 16-layer CNN-LSTM model for binary classification of MI using one-lead ECG data [83]. During pre-processing, they used the wavelet transform method to filter the original ECG noise and the Daubechies wavelet basis function to decompose the ECG signals into 10 levels. They used the Pan–Tompkins algorithm to detect the R-peaks in ECG recordings, which were then utilized for heartbeat segmentation to a fixed length. Since the ECG data were not balanced, they performed random over-sampling to avoid over-fitting during training and improve the model's generalizability. They trained the CNN-LSTM model to automatically learn spatial and temporal characteristics of ECG signals. They observed that the model achieved the highest accuracy when the data of five adjacent heartbeats were selected as the input and the Adam optimizer was utilized. They obtained an accuracy of 95.4 %, sensitivity of 98.2 %, specificity of 86.5 %, and F1-score of 96.8 %.

Rath et al. used four deep learning models, including autoencoder, RBM, SOM, and radial basis function network (RBFN), to detect CAD using ECG signals [64]. Additionally, they developed an ensemble model by combining the two

best-performing deep learning models, which were autoencoder and SOM models, based on the principle of majority voting. The order of performance rankings for CAD detection, from the highest to the lowest, belonged to the SOM-autoencoder, autoencoder, SOM, RBFN, and RBM models, respectively. Hence, the SOM-autoencoder ensemble model outperformed all individual deep learning models with an accuracy of 98.4 % and F1-score of 97.1 %. They asserted that this could be attributed to the ensemble model's ability to overcome the statistical, computational, and representational problems associated with the datasets.

Prabhakararao et al. introduced an end-to-end multi-lead diagnostic attention-based RNN (MLDA-RNN) for automated diagnosis of the three MI severity stages from healthy control subjects [80]. They employed RNNs to encode the temporal variations in the 12-lead ECG signals. These encoded vectors from the RNN encoding blocks were fed to the intra-lead attention module to summarize the within-lead discriminative vectors and obtain lead-attentive representations. Then, the inter-lead attention module aggregated these representative vectors from the intra-lead attention module based on their clinical relevance to obtain a high-level feature representation for reliable diagnosis. The vector obtained from the inter-lead attention module was fed to the fully connected layer with a softmax activation function to classify the MI severity stages. They employed batch normalization layers after the inter-lead attention module to improve the speed of convergence. They used a dropout layer before the output layer to improve the model generalization. They trained the model using back-propagation through time (BPTT) and they employed early stopping method to avoid over-fitting. They utilized the grid search method to optimize the hyper-parameters of the RNN and attention modules. The model exhibited an overall accuracy of 97.7 %, sensitivity of 97.6 %, and specificity of 99.4 % without compromising on the class-wise detection rates. They claimed that MLDA-RNN showed promising results for model interpretability, as the learned attention weights often correlated with the clinicians' way of diagnosing MI severity stages.

Hernandez et al. proposed an automated method for the detection of MI from continuous ECG monitoring using a set of ECG and VCG features [81]. First, they applied a median filter to remove high-frequency noise. Next, they implemented a moving window over the filtered signal and calculated the distribution parameter values in each window. They selected the optimal distribution parameters by performing a statistical analysis to control the model's complexity, prevent over-fitting, and facilitate the model's learning process. From this, they obtained another time-series for each distribution parameter. They derived seven ECG features from VCG, which were found to be optimal for detecting MI using the reduced 3-lead ECG signals. Out of the seven ECG features, five were VCG features derived from the QRS and T wave complexes, while the other two were ST elevation features. They analyzed the distribution properties of each ECG feature to facilitate the identification of underlying patterns in the data. They used these features to train and validate the RNN that was composed of two unidirectional LSTMs with a fully connected layer and ReLU activation function. They observed a clear separation in ECG feature median values between the baseline and MI conditions for the two distribution parameters, indicating that these may be suitable parameters for characterizing MI. The proposed method had an accuracy of 97.4 % and sensitivity of 94.7 %. The drawback of this study is the use of a reduced number of ECG leads, which can limit the detection performance of certain types of MI.

Miao et al. presented an enhanced DNN model for the diagnosis and prognosis of CAD [86]. The proposed DNN model includes two hidden layers and an output layer with a sigmoid activation function. It was built based on a deep MLP architecture equipped with linear and non-linear transfer functions, regularization, dropout, and a binary classification layer. During the training of the DNN, the dropout rates in both hidden layers were randomly applied, resulting in random connections within the DNN architecture to reduce over-fitting. The model had an accuracy of 83.6 %, sensitivity of 93.5 %, specificity of 72.8 %, precision of 79.1 %, and F1-score of 85.7 %. The limitation of this study is that they did not use cross-validation to ensure robustness.

Bigler et al. introduced a CNN trained with transfer learning to perform binary classification for ISC diagnosis using one-lead ECG images [3]. They conducted a retrospective observational study to test a hypothesis-generating approach using an open-access CNN model with different depth and network architecture that was pretrained using the images on the ImageNet dataset. Before training the CNN on this study's database, all training images were randomly shuffled and processed by adding noise to prevent over-fitting. The underlying morphology responsible for the network prediction for ISC detection focused mainly on the distinctive features in the ST-segment and T-wave of ECG. During transfer learning, the last three layers of the CNN responsible for the network prediction were replaced for the new task. Remaining layers responsible for pattern recognition and feature extraction were not changed. A dropout layer was added to prevent the CNN from over-fitting. The CNN showed a sensitivity of 83 %, specificity of 98 %, accuracy of 91.5 %, and F1-score of 89.9 %, which revealed higher performance than manually obtained quantitative intracoronary ECG ST-segment shift for ISC detection.

Altan et al. suggested a decision-support system to aid cardiologists in CAD diagnosis [33]. Firstly, short-term ECG segments were randomly obtained from 24-hour ECG signals using the moving window analysis technique to increase the number of samples from each subject. In the first stage of the Hilbert-Huang Transform, frequency-modulated signals, named intrinsic mode functions, were extracted by applying empirical mode decomposition (EMD) to short-term ECG segments. In the second stage, the Hilbert Transform was applied to each intrinsic mode function to calculate the instantaneous frequency spectral features. The binary classification using the statistical features of intrinsic mode functions was performed using a DBN classifier, which had one input layer, two hidden layers, and one output layer with two outputs for binary classification. The DBN classifier first evaluates weights and biases between visible and hidden layers using an unsupervised pre-training of stacked RBMs. Next, in the supervised learning phase, weights and biases were updated using fine-tuning to optimize the parameters for improving classification performance. The activation functions of the hidden and output layers in the supervised learning phase were the hyperbolic tangent and sigmoid functions, respectively. The DBN classifier had an accuracy of 98 %, specificity of 98.8 %, and sensitivity of 96 % using the 10-fold cross-validation method.

Xiao et al. explored the application of CNN to detect significant changes in the ST segments of whole-day Holter ECG signals for CAD diagnosis [68]. They generated image-based samples by taking 10-second snapshots of one-lead ECG waveforms and transforming them into grayscale images using a grid overlay to remove redundant color information that does not contribute to the classification task. These images were then saved as 8-bit JPEG files and resized using bilinear interpolation to adhere to the input requirements of the Google Inception V3 model, which had been pre-trained using transfer learning from the images in the ImageNet dataset. The image features that differentiate ST from non-ST conditions were extracted by the convolutional layers in the CNN model for the classification of each 10-second image sample. They kept all the model parameters in the Google Inception V3 model, except for the final layer that was retrained using the training images in the present study. The model exhibited a sensitivity of 82.6 %, specificity of 80.3 %, and F1-score of 87.3 %. It achieved comparable performance to that of expert cardiologists in detecting ST changes. The limitation of the study is that the algorithm was built upon one-lead ECG data.

Butun et al. proposed a computer-aided diagnosis system with a 1D capsule network (1D-CapsNet) for automated detection of CAD from short-length ECG segments [85]. First, they applied DWT to raw ECG signals to eliminate noise. Subsequently, they used Z-score normalization to make the ECG signals suitable for input to the proposed network. They modified the original capsule network model for 1D signal applications by redefining the layer parameters and adding some sub-layers to detect CAD. They employed two ECG capsules that represented the normal and CAD classes. The decoder section of the capsule networks compressed the ECG signals and acted as a regulator for the protection of important features in the capsule layers during training. The model yielded an accuracy of 98.6 %, sensitivity of 97.9 %, specificity of 98.7 %, and precision of 93.3 % for short-length ECG segments using 5-fold cross-validation method. They asserted that the model can be used as a diagnostic tool to assist cardiologists during medical examinations by providing a second opinion on the patient's condition.

Acharya et al. utilized a 1D-CNN structure for the diagnosis of CAD using short-length ECG segments [12]. First, they applied DWT to the ECG segments to eliminate noise. Subsequently, they used z-score normalization to normalize the ECG segments. They developed an 11-layered CNN structure, including four convolutional layers, four max-pooling layers, and three fully connected layers, to perform binary classification. The 1D-CNN was able to differentiate between normal and abnormal ECG with an accuracy of 95.1 %, sensitivity of 91.1 %, specificity of 95.8 %, and precision of 80.8 %. They claimed that the proposed CNN structure was robust to shifting and scaling invariance, and that the proposed system is suitable for real-time monitoring.

Dutta et al. presented a simple 2-layer CNN that is resistant to class imbalance and performs binary classification on significantly class imbalanced ECG data for CAD diagnosis [72]. Data preprocessing was performed using least absolute shrinkage and selection operator (LASSO) based feature weight assessment. LASSO regression was performed repeatedly using multiple instances of randomly subsampled datasets to assess the consistency of the attribute contributions. A majority-voting algorithm was applied to extract the important features and identify the contribution of significant attributes in the data variation, which provides dimensionality reduction by excising unimportant variables. Subsequently, the important features were fed to the 1D-CNN and then homogenized using a fully connected layer. They employed a simulated annealing-like training schedule to minimize the generalization error between train and test losses. The nonlinear transformation was performed using ReLU and dropout was applied to reduce over-fitting. The shallow CNN architecture demonstrated a classification power of 77 % in correctly classifying the presence of CAD on the test set. The recall values of other machine learning methods, such as SVM and random forest, were comparable to that of the CNN model. However, the

accuracy of CNN (79.5 %) was better than individual accuracies of SVM or random forest classifiers and CNN predicted the negative (non-CAD) cases with higher accuracy. They asserted that the CNN exhibited a considerable degree of resilience towards data imbalance.

Sharma et al. presented a rhythm-based methodology for the point-of-care diagnosis of CARs at a primary level [40]. During pre-processing, the frequency normalization was performed to match the sampling frequency of the datasets from different sources to the input of the proposed algorithm. Therefore, the three databases were down-sampled to 300 Hz to maintain homogeneity with the training data and the algorithm. A Butterworth band-pass filter was employed to eliminate the baseline drift and high frequency noise from one-lead ECG signals. A dataset dependent notch filter with an appropriate frequency of either 50 Hz or 60 Hz was used to remove the power-line interference. The QRS detection algorithm was applied to the filtered ECG signals, and the RR-interval sequences of one-lead and short-length ECG segments were computed. Fourier-Bessel sequences were calculated using the FBSE to transform the RR-interval sequences into more meaningful sequences that can better characterize the cardiac rhythms into normal and abnormal classes. The computed Fourier-Bessel coefficients of different lengths for different subjects were upsampled to a fixed number to make Fourier-Bessel sequences homogeneous in terms of length. The derived Fourier-Bessel sequences-based intelligent series were used as input to the unidirectional LSTM model, which was used to directly extract significant information required for binary classification. They obtained an accuracy of 78.4 %, sensitivity of 65.1 %, specificity of 86.8 %, and F1-score of 76.5 % in classifying normal and CAR classes using 10-fold cross-validation. They claimed that the addition of the FBSE-layer improved CAR detection performance, and that the proposed intelligent series can reveal the differences between normal and CAR ECG signals.

The performance of the automated AIHAD technique is better than that of most previously proposed deep learning approaches that exclusively used ECG data to diagnose or classify CADs. Specifically, the binary classification performance results of the automated AIHAD technique on the PTBD database showed that the technique has higher sensitivity (TPR), higher specificity (TNR), higher F_1-score (F1), higher precision (PPV), higher accuracy (ACC), and higher negative predictive value (NPV) compared to most of the existing studies in the literature that utilized deep learning methods and only ECG data to diagnose or classify CADs (Table 18).

However, a few studies in the literature that used machine or deep learning approaches and only ECG data demonstrated slightly better performance compared to our proposed automated AIHAD technique [28, 29, 39, 41, 85]. This is a highly anticipated result, since deep learning methods often work with larger amounts of data, which improves their performance results. Moreover, they can benefit from transfer learning, in which they are pretrained on significantly larger databases and then fine-tuned on the specific database of interest. Additionally, some of these existing studies [39, 85] were developed and evaluated on different databases, which may have contributed to their slightly better performance results. Although these few existing studies [28, 29, 41] achieved slightly better performance, our results are still highly competitive.

Compared to existing related methods, one of the biggest advantages of the proposed automated AIHAD technique is that it can provide accurate and reliable diagnosis of AISC, which was one of the aims and motivations of this study. Therefore, the AIHAD technique targets to address the limitations of existing related studies that have used only ECG data to detect CADs and fill the research gaps in the literature. Thus, the automated AIHAD technique can be highly beneficial and valuable by providing improved diagnosis, particularly for asymptomatic CAD patients with AISC, for whom the diagnostic information provided by ECG alone is not sufficient to reliably diagnose the disease.

Another advantage of the proposed AIHAD technique, over some of the existing machine and deep learning methods, is that it can automatically process all 12-leads for enhanced CAD diagnosis, instead of only one-lead. This is particularly important as each lead provides diagnostic information about the heart from a different angle, and multiple leads are required for the accurate and reliable diagnosis of CADs [1, 4, 7, 8, 11, 28, 29, 53, 110]. Therefore, the automated AIHAD technique benefits from the diversity in diagnostic information provided by all 12-leads and can accurately detect CAD cases that cannot be diagnosed using only one-lead. This advantage may have substantially contributed to the relatively higher performance of the automated AIHAD technique on the STAFF III and PTBD databases.

Conversely, either one-lead or a limited number of leads was used to diagnose or classify CADs in some of the existing methods in Tables 17 and 18 [12, 28, 39, 40, 44, 56, 67, 68, 71, 75, 77, 81, 83, 85, 88]. However, certain types of CADs are lead-specific and can only be detected through particular leads. Consequently, they might be missed by methods that monitor only one-lead or a very few number of leads. This limitation may result in poor generalization and these existing methods may not provide a reliable diagnosis for CADs that are localized in various heart locations [1, 4, 7, 8, 11, 28, 29, 53, 110].

Table 18: The performance comparison between the proposed automated AIHAD technique and recent deep learning studies that used only ECG data for CAD diagnosis or classification.

Study	Technique	Database	TPR (%)	TNR (%)	PPV (%)	F1 (%)	ACC (%)	NPV (%)
Brisk et al. [73]	CNN	STAFF III database	84.2	94.7	–	81.4	80.3	–
Proposed method	**AIHAD**	**STAFF III database**	**96.21**	**93.18**	**93.38**	**94.78**	**94.70**	**96.09**
Reasat et al. [71]	CNN	PTBD database	85.3	84.1	–	–	84.5	–
Makimoto et al. [74]	CNN	PTBD database	65	86	82	72	75	71
Hammad et al. [75]	CNN	PTBD database	81.1	–	88.5	83	89.7	–
Darmawahyuni et al. [82]	RNN	PTBD database	98.4	97.9	95.6	96.3	–	–
Feng et al. [83]	CNN-RNN	PTBD database	98.2	86.5	–	96.8	95.4	–
Rath et al. [64]	SOM-autoencoder	PTBD database	–	–	–	97.1	98.4	–
Proposed method	**AIHAD**	**PTBD database**	**98.48**	**97.73**	**97.74**	**98.11**	**98.11**	**98.47**
Prabhakararao et al. [80]	RNN	PhysioNet database	97.6	99.4	–	–	97.7	–
Hernandez et al. [81]	RNN	PhysioNet database	94.7	–	–	–	97.4	–
Miao et al. [86]	DNN	UCI machine learning repository	93.5	72.8	79.1	85.7	83.6	–
Bigler et al. [3]	CNN	Self-collected ECG data	83	98	–	89.9	91.5	–
Altan et al. [33]	DBN	Long-term ST database	96	98.8	–	–	98	–
Xiao et al. [68]	CNN	Long-term ST database	82.6	80.3	–	87.3	–	–
Butun et al. [85]	1D-CADCapsNet	St. Petersburg ICT database	97.9	98.7	93.3	–	98.6	–
Acharya et al. [12]	CNN	St. Petersburg ICT database	91.1	95.8	80.8	–	95.1	–
Dutta et al. [72]	CNN	Nhanes database	77	–	–	–	79.5	–
Sharma et al. [40]	LSTM	MIT-BIH database	65.1	86.8	–	76.5	78.4	–

Another advantage of the automated AIHAD technique is its very short implementation time, which is highly desirable for real-time detection of CADs. This may support fast decision-making by physicians in clinical settings, which could have significant implications in emergency situations where rapid diagnosis is crucial for timely patient treatment.

Furthermore, the advantage of the automated AIHAD technique over the microneurography technique, which is the conventional method for invasively recording and monitoring SNS activities, is that it uses wideband recordings non-invasively acquired from patients to detect CSNA. Thus, it significantly reduces the risks associated with invasive procedures and the limitations associated with the requirement of highly specialized skills and expertise from trained clinicians, while also improving patient comfort.

Moreover, in clinical practice, two different physicians can often make inconsistently different diagnoses for the same patient successively [9, 11, 53, 85]. An important advantage of the automated AIHAD technique is its ability to provide the patient with consistently accurate diagnoses successively.

Additionally, two publicly available databases were used for the development and evaluation of the automated AIHAD technique. The results obtained on both databases using the automated AIHAD technique strongly support each other. The consistently high performance results of the AIHAD technique on two different databases that contain different and diverse patients with CADs indicate that the technique is quite robust and generalizable.

The common drawback of most previously proposed AI studies that investigated the diagnosis or classification of CADs is that they only utilized ECG data [3–9, 11, 12, 15, 17, 19–30, 32–37, 39, 41–45, 48, 49, 51–61, 64–69, 71–88, 94–97, 109, 110]. To the best of our knowledge, this is the first study that proposes a hybrid AI technique that jointly and simultaneously analyzes 12-lead CSNA and ECG data to provide fast, early, and accurate diagnosis of a heart disease. Since, there are no other studies in the literature that proposed a hybrid AI technique that jointly uses CSNA and ECG data or separately uses only CSNA data to diagnose or classify CVDs, it is not possible to compare the performance results of the proposed automated AIHAD technique with those of other studies.

Conclusions and future work

This study presents a novel automated hybrid AI technique that simultaneously and robustly detects anomalies in the 12-lead CSNA and ECG data for fast, early, and accurate diagnosis of CADs. We evaluated the performance and generalizability of the proposed AIHAD technique on the fully-labeled STAFF III and PTBD databases. The experimental results have shown that the automated AIHAD technique

yields very promising results for the reliable and robust detection of CADs from the 12-lead ECG and CSNA data.

In the future, we will embed the automated AIHAD technique in hospitals' software systems and clinically validate it through multi-center prospective studies to demonstrate its high performance, generalizability, and robustness on a larger and more diverse patient population, as well as to determine the amount of time it saves physicians in daily clinical practice.

After ensuring its reliability for widespread clinical applicability, it may be integrated into wearable devices, such as wireless patches and smartwatches, for continuous, simultaneous, and long-term monitoring of CSNA and ECG in real-time. In this way, it may provide early warnings to the patients for early diagnosis and treatment of CADs, which highlights the potential benefits of this study in real-world medical scenarios.

Consequently, it may serve as an efficient decision-support system to increase the success of physicians in fast, early, and accurate diagnosis of CADs. This can help reduce the risk of misdiagnosis by human experts and aid physicians in making informed diagnostic decisions efficiently. Therefore, the contribution of the automated AIHAD technique to the reliable diagnosis of CADs can be much higher than that of conventional ECG devices and the utilization of CSNA in the diagnosis of CVDs can gain a new perspective.

Ethical approval: Not applicable.
Informed consent: Not applicable.
Author contributions: Authors have accepted responsibility for the entire content of this manuscript and approved its submission.
Competing interests: Authors state no conflict of interest.
Research funding: None declared.

References

1. Virani SS, Alonso A, Aparicio HJ, Benjamin EJ, Bittencourt MS, Callaway CW, et al. Heart disease and stroke statistics-2021 update: a report from the American Heart Association. Circulation 2021;143:e254–743.
2. Wang JJ, Pahlm O, Warren JW, Sapp JL, Horáček BM, et al. Criteria for ECG detection of acute myocardial ischemia: sensitivity versus specificity. J Electrocardiol 2018;51:S12–7.
3. Bigler MR, Seiler C. Detection of myocardial ischemia by intracoronary ECG using convolutional neural networks. PLOS ONE 2021;16:1–17.
4. Sun Q, Liang C, Chen T, Ji B, Liu R, Wang L, et al. Early detection of myocardial ischemia in 12-lead ECG using deterministic learning and ensemble learning. Comput Method Progr Biomed 2022;226:107124. 107124.
5. Song J, Yan H, Xu Z, Yu X, Zhu R. Myocardial ischemia analysis based on electrocardiogram QRS complex. Australas Phys Eng Sci Med 2011;34: 515–21.
6. Martis RJ, Chakraborty C, Ray AK. A two-stage mechanism for registration and classification of ECG using Gaussian mixture model. Pattern Recogn 2009;42:2979–88.
7. Cairns AW, Bond RR, Finlay DD, Guldenring D, Badilini F, Libretti G, et al. A decision support system and rule-based algorithm to augment the human interpretation of the 12-lead electrocardiogram. J Electrocardiol 2017;50:781–6.
8. Dohare AK, Kumar V, Kumar R. Detection of myocardial infarction in 12 lead ECG using support vector machine. Appl Soft Comput 2018;64: 138–47.
9. Savostin AA, Ritter DV, Savostina GV. Using the k-nearest neighbors algorithm for automated detection of myocardial infarction by electrocardiogram data entries. Pattern Recogn Image Anal 2019;29: 730–7.
10. Berikol GB, Yildiz O, Özcan IT. Diagnosis of acute coronary syndrome with a support vector machine. J Med Syst 2016;40:84.
11. Al-Zaiti S, Besomi L, Bouzid Z, Faramand Z, Frisch S, Martin-Gill C, et al. Machine learning-based prediction of acute coronary syndrome using only the pre-hospital 12-lead electrocardiogram. Nat Commun 2020; 11:3966.
12. Acharya UR, Fujita H, Lih OS, Adam M, Tan JH, Chua CK. Automated detection of coronary artery disease using different durations of ECG segments with convolutional neural network. Knowl Base Syst 2017; 132:62–71.
13. Hart EC, Head GA, Carter JR, Wallin BG, May CN, Hamza SM, et al. Guidelines in cardiovascular research: recording sympathetic nerve activity in conscious humans and other mammals: guidelines and the road to standardization. Am J Physiol Heart Circ Physiol 2017;312: H1031–51.
14. Zhang P, Liang JJ, Cai C, Tian Y, Dai MY, Wong J, et al. Characterization of skin sympathetic nerve activity in patients with cardiomyopathy and ventricular arrhythmia. Heart Rhythm 2019;16:1669–75.
15. Gomis P, Caminal P, Vallverdu M, Warren S, Wagner G. Non-linear dynamic analysis of the cardiac rhythm during transient myocardial ischemia. Biomed Eng/ Biomed Tech 2006;51:178–81.
16. Kusayama T, Wan J, Doytchinova A, Wong J, Kabir RA, Mitscher G, et al. Skin sympathetic nerve activity and the temporal clustering of cardiac arrhythmias. JCI Insight 2019;4. https://doi.org/10.1172/jci.insight. 125853.
17. Ortigosa N, Fernández C, Galbis A, Cano O. Classification of persistent and long-standing persistent atrial fibrillation by means of surface electrocardiograms. Biomed Eng/Biomed Tech 2016;61:19–27.
18. Mateo C, Talavera JA. Analysis of atrial and ventricular premature contractions using the short time Fourier transform with the window size fixed in the frequency domain. Biomed Signal Process Control 2021;69:102835.
19. Ertuğrul ÖF, Acar E, Aldemir E, Öztekin A. Automatic diagnosis of cardiovascular disorders by sub images of the ECG signal using multi-feature extraction methods and randomized neural network. Biomed Signal Process Control 2021;64:102260.
20. Li H, An Z, Zuo S, Zhu W, Cao L, Mu Y, et al. Classification of electrocardiogram signals with waveform morphological analysis and support vector machines. Med Biol Eng Comput 2022;60: 109–19.
21. Kumari LV, Sai YP. Classification of ECG beats using optimized decision tree and adaptive boosted optimized decision tree. Signal Image Video Process 2022;16:695–703.
22. Kalidas V, Tamil LS. Detection of atrial fibrillation using discrete-state Markov models and random forests. Comput Biol Med 2019;113: 103386.

23. Alqudah AM, Albadarneh A, Abu-Qasmieh I, Alquran H. Developing of robust and high accurate ECG beat classification by combining Gaussian mixtures and wavelets features. Australas Phys Eng Sci Med 2019;42:149–57.
24. Singh P, Pradhan G. Noise robust automatic heartbeat classification system using support vector machine and conditional spectral moment. Phys Eng Sci Med 2020;43:1387–98.
25. Sahoo S, Kanungo B, Behera S, Sabut S. Multiresolution wavelet transform based feature extraction and ECG classification to detect cardiac abnormalities. Measurement 2017;108:55–66.
26. Sabut S, Pandey O, Mishra BS, Mohanty M. Detection of ventricular arrhythmia using hybrid time–frequency-based features and deep neural network. Phys Eng Sci Med 2021;44:135–45.
27. Acharya UR, Fujita H, Adam M, Lih OS, Sudarshan VK, Hong TJ, et al. Automated characterization and classification of coronary artery disease and myocardial infarction by decomposition of ECG signals: a comparative study. Inf Sci 2017;377:17–29.
28. Sharma LD, Sunkaria RK. Myocardial infarction detection and localization using optimal features based lead specific approach. IRBM 2020;41:58–70.
29. Acharya UR, Fujita H, Sudarshan VK, Oh SL, Adam M, Koh JE, et al. Automated detection and localization of myocardial infarction using electrocardiogram: a comparative study of different leads. Knowl Base Syst 2016;99:146–56.
30. Yanık H, Değirmenci E, Büyükakıllı B, Karpuz D, Kılınç OH, Gürgül S. Electrocardiography (ECG) analysis and a new feature extraction method using wavelet transform with scalogram analysis. Biomed Eng/Biomed Tech 2020;65:543–56.
31. Eltrass AS, Tayel MB, Ammar AI. A new automated CNN deep learning approach for identification of ECG congestive heart failure and arrhythmia using constant-Q non-stationary Gabor transform. Biomed Signal Process Control 2021;65:102326.
32. Acharya UR, Fujita H, Sudarshan VK, Oh SL, Adam M, Tan JH, et al. Automated characterization of coronary artery disease, myocardial infarction, and congestive heart failure using contourlet and shearlet transforms of electrocardiogram signal. Knowl Base Syst 2017;132:156–66.
33. Altan G. Diagnosis of coronary artery disease using deep belief networks. Eur J Eng Nat Sci 2017;2:29–36.
34. Chang KM. Ensemble empirical mode decomposition for high frequency ECG noise reduction. Biomed Eng/Biomed Tech 2010;55:193–201.
35. Raj S, Ray KC, Shankar O. Cardiac arrhythmia beat classification using DOST and PSO tuned SVM. Comput Methods Progr Biomed 2016;136: 163–77.
36. Rajesh KNVPS, Dhuli R. Classification of ECG heartbeats using nonlinear decomposition methods and support vector machine. Comput Biol Med 2017;87:271–84.
37. Shafi I, Aziz A, Din S, Ashraf I. Reduced features set neural network approach based on high-resolution time-frequency images for cardiac abnormality detection. Comput Biol Med 2022;145:105425.
38. Chaudhary PK, Gupta V, Pachori RB. Fourier-Bessel representation for signal processing: a review. Digit Signal Process 2023;135:103938.
39. Ramasamy K, Balakrishnan K, Velusamy D. Detection of cardiac arrhythmias from ECG signals using FBSE and jaya optimized ensemble random subspace K-nearest neighbor algorithm. Biomed Signal Process Control 2022;76:103654.
40. Sharma A, Garg N, Patidar S, San Tan R, Acharya UR. Automated pre-screening of arrhythmia using hybrid combination of Fourier–Bessel expansion and LSTM. Comput Biol Med 2020;120:103753.
41. Tripathy RK, Bhattacharyya A, Pachori RB. A novel approach for detection of myocardial infarction from ECG signals of multiple electrodes. IEEE Sensor J 2019;19:4509–17.
42. Jayasanthi M, Rajendran G, Vidhyakar RB. Independent component analysis with learning algorithm for electrocardiogram feature extraction and classification. Signal Image Video Process 2021;15:391–9.
43. Castells F, Cebrián A, Millet J. The role of independent component analysis in the signal processing of ECG recordings. Biomed Eng/ Biomed Tech 2007;52:18–24.
44. Sadhukhan D, Pal S, Mitra M. Automated identification of myocardial infarction using harmonic phase distribution pattern of ECG data. IEEE Trans Instrum Meas 2018;67:2303–13.
45. Green M, Björk J, Forberg J, Ekelund U, Edenbrandt L, Ohlsson M. Comparison between neural networks and multiple logistic regression to predict acute coronary syndrome in the emergency room. Artif Intell Med 2006;38:305–18.
46. Ghiasi MM, Zendehboudi S, Mohsenipour AA. Decision tree-based diagnosis of coronary artery disease: CART model. Comput Methods Progr Biomed 2020;192:105400.
47. Neha, SHK, Kanwade R, Tewary S. Arrhythmia detection and classification using ECG and PPG techniques: a review. Phys Eng Sci Med 2021;44:1–22.
48. Yang W, Si Y, Wang D, Guo B. Automatic recognition of arrhythmia based on principal component analysis network and linear support vector machine. Comput Biol Med 2018;101:22–32.
49. Agrawal RK, Sewani RR, Delen D, Benjamin B. A machine learning approach for classifying healthy and infarcted patients using heart rate variabilities derived vector magnitude. Healthcare Analytics 2022; 2:100121. 100121.
50. Chakir F, Jilbab A, Nacir C, Hammouch A. Recognition of cardiac abnormalities from synchronized ECG and PCG signals. Phys Eng Sci Med 2020;43:673–7.
51. Jothiramalingam R, Anitha J, Hemanth DJ. Diagnosis of coronary artery occlusion by fitting polynomial curve with the ECG signal based on optimization techniques. Netw Model Anal Health Inform Bioinform 2022;11:16.
52. Huo R, Zhang L, Liu F, Wang Y, Liang Y, Wei S. ECG segmentation algorithm based on bidirectional hidden semi-Markov model. Comput Biol Med 2022;150:106081.
53. Chang PC, Lin JJ, Hsieh JC, Weng J. Myocardial infarction classification with multi-lead ECG using hidden Markov models and Gaussian mixture models. Appl Soft Comput 2012;12:3165–75.
54. Ojha MK, Wadhwani S, Wadhwani AK, Shukla A. Automatic detection of arrhythmias from an ECG signal using an auto-encoder and SVM classifier. Phys Eng Sci Med 2022;45:665–74.
55. Hamil H, Zidelmal Z, Azzaz MS, Sakhi S, Kaibou R, Ould Abdeslam D. Afepisodes recognition using optimized time-frequency features and cost-sensitive SVM. Phys Eng Sci Med 2021;44:613–24.
56. Ahmad Z, Tabassum A, Guan L, Khan NM. ECG heartbeat classification using multimodal fusion. IEEE Access 2021;9:100615–26.
57. Magrans R, Gomis P, Caminal P. Myocardial ischemia event detection based on support vector machine model using QRS and ST segment features. In 2016 Computing in Cardiology Conference (CinC) 2016: 405–8 pp.
58. Yang P, Wang D, Zhao WB, Fu LH, Du JL, Su H. Ensemble of kernel extreme learning machine based random forest classifiers for automatic heartbeat classification. Biomed Signal Process Control 2021;63:102138.

59. Sraitih M, Jabrane Y, Hajjam El Hassani A. A robustness evaluation of machine learning algorithms for ECG myocardial infarction detection. J Clin Med 2022;11:4935.
60. Bashir S, Qamar U, Khan FH. A multicriteria weighted vote-based classifier ensemble for heart disease prediction. Comput Intell 2016; 32:615–45.
61. Daraei A, Hamidi H. An efficient predictive model for myocardial infarction using cost-sensitive j48 model. Iran J Public Health 2017;46: 682.
62. De La Fuente-Cortes G, Diaz-Mendez A, Gonzalez-Diaz VR. A fully integrated fuzzy logic algorithm for ischemic heartbeat classification. In 2018 25th IEEE International Conference on Electronics, Circuits and Systems (ICECS); 2018:873–6 pp.
63. Lee M, Song TG, Lee JH. Heartbeat classification using local transform pattern feature and hybrid neural fuzzy-logic system based on self-organizing map. Biomed Signal Process Control 2020;57:101690.
64. Rath A, Mishra D, Panda G, Satapathy SC, Xia K. Improved heart disease detection from ECG signal using deep learning based ensemble model. Sustain Comput Inform Syst 2022;35:100732.
65. Javadi M, Arani SA, Sajedin A, Ebrahimpour R. Classification of ECG arrhythmia by a modular neural network based on Mixture of Experts and Negatively Correlated Learning. Biomed Signal Process Control 2013;8:289–96.
66. Ebrahimpour R, Sadeghnejad N, Sajedin A, Mohammadi N. Electrocardiogram beat classification via coupled boosting by filtering and preloaded mixture of experts. Neural Comput Appl 2013;23:1169–78.
67. Exarchos TP, Papaloukas C, Fotiadis DI, Michalis LK. An association rule mining-based methodology for automated detection of ischemic ECG beats. IEEE Trans Biomed Eng 2006;53:1531–40.
68. Xiao R, Xu Y, Pelter MM, Fidler R, Badilini F, Mortara DW, et al. Monitoring significant ST changes through deep learning. J Electrocardiol 2018;51:S78–82.
69. Meng L, Ge K, Song Y, Yang D, Lin Z. Long-term wearable electrocardiogram signal monitoring and analysis based on convolutional neural network. IEEE Trans Instrum Meas 2021;70:1–11.
70. Pandey SK, Janghel RR. Automatic detection of arrhythmia from imbalanced ECG database using CNN model with SMOTE. Australas Phys Eng Sci Med 2019;42:1129–39.
71. Reasat T, Shahnaz C. Detection of inferior myocardial infarction using shallow convolutional neural networks. In 2017 IEEE region 10 humanitarian technology conference (R10-HTC); 2017:718–21 pp.
72. Dutta A, Batabyal T, Basu M, Acton ST. An efficient convolutional neural network for coronary heart disease prediction. Expert Syst Appl 2020;159:113408.
73. Brisk R, Bond R, Finlay D, McLaughlin J, Piadlo A, Leslie SJ, et al. The effect of confounding data features on a deep learning algorithm to predict complete coronary occlusion in a retrospective observational setting. Eur Heart J Digit Health 2021;2:127–34.
74. Makimoto H, Höckmann M, Lin T, Glöckner D, Gerguri S, Clasen L, et al. Performance of a convolutional neural network derived from an ECG database in recognizing myocardial infarction. Sci Rep 2020;10:8445.
75. Hammad M, Alkinani MH, Gupta BB, Abd El-Latif AA. Myocardial infarction detection based on deep neural network on imbalanced data. Multimed Syst 2022;28:1373–85.
76. Warrick PA, Homsi MN. Ensembling convolutional and long short-term memory networks for electrocardiogram arrhythmia detection. Physiol Meas 2018;39:114002.
77. Martin H, Izquierdo W, Cabrerizo M, Cabrera A, Adjouadi M. Near real-time single-beat myocardial infarction detection from single-lead electrocardiogram using long short-term memory neural network. Biomed Signal Process Control 2021;68:102683.
78. Liu P, Sun X, Han Y, He Z, Zhang W, Wu C. Arrhythmia classification of LSTM autoencoder based on time series anomaly detection. Biomed Signal Process Control 2022;71:103228.
79. Pandey SK, Janghel RR. Automated detection of arrhythmia from electrocardiogram signal based on new convolutional encoded features with bidirectional long short-term memory network classifier. Phys Eng Sci Med 2021;44:173–82.
80. Prabhakararao E, Dandapat S. Myocardial infarction severity stages classification from ECG signals using attentional recurrent neural network. IEEE Sensor J 2020;20:8711–20.
81. Hernandez AA, Bonizzi P, Peeters R, Karel J. Continuous monitoring of acute myocardial infarction with a 3-lead ECG system. Biomed Signal Process Control 2023;79:104041.
82. Darmawahyuni A, Nurmaini S, Sukemi, Caesarendra W, Bhayyu V, Rachmatullah MN, et al. Deep learning with a recurrent network structure in the sequence modeling of imbalanced data for ECG-rhythm classifier. Algorithms 2019;12:118.
83. Feng K, Pi X, Liu H, Sun K. Myocardial infarction classification based on convolutional neural network and recurrent neural network. Appl Sci 2019;9:1879.
84. Lih OS, Jahmunah V, San TR, Ciaccio EJ, Yamakawa T, Tanabe M, et al. Comprehensive electrocardiographic diagnosis based on deep learning. Artif Intell Med 2020;103:101789.
85. Butun E, Yildirim O, Talo M, Tan RS, Acharya UR. 1D-CADCapsNet: one dimensional deep capsule networks for coronary artery disease detection using ECG signals. Phys Med 2020;70:39–48.
86. Miao KH, Miao JH. Coronary heart disease diagnosis using deep neural networks. Int J Adv Comput Sci Appl 2018;9. https://doi.org/10.14569/IJACSA.2018.091001.
87. Samann F, Schanze T. Multiple ECG segments denoising autoencoder model. Biomed Eng/Biomed Tech 2023;68:275–84.
88. Yan Y, Qin X, Wu Y, Zhang N, Fan J, Wang L. A restricted Boltzmann machine based two-lead electrocardiography classification. In 2015 IEEE 12th International conference on wearable and implantable body sensor networks (BSN); 2015:1–9.
89. Laguna P, Sörnmo L. The STAFF III ECG database and its significance for methodological development and evaluation. J Electrocardiol 2014;47:408–17.
90. Goldberger AL, Amaral LA, Glass L, Hausdorff JM, Ivanov PC, Mark RG, et al. Physio bank, physiotoolkit, and physionet: components of a new research resource for complex physiologic signals. Circulation 2000; 101:e215-20.
91. Bousseljot R, Kreiseler D, Schnabel A. Nutzung der EKG-Signaldatenbank CARDIODAT der PTB über das. Biomed Eng/Biomed Technik 1995;40:317–8.
92. Oeff M, Koch H, Bousseljot R, Kreiseler D. The PTB diagnostic ECG database. Braunschweig, Germany: National Metrology Institute of Germany; 2012.
93. Rahul J, Sharma LD, Bohat VK. Short duration vectorcardiogram based inferior myocardial infarction detection: class and subject-oriented approach. Biomed Eng/Biomed Tech 2021;66:489–501.
94. Raj S, Ray KC, Shankar O. Development of robust, fast and efficient QRS complex detector: a methodological review. Australas Phys Eng Sci Med 2018;41:581–600.
95. Rahul J, Sora M, Sharma LD. Exploratory data analysis based efficient QRS-complex detection technique with minimal computational load. Phys Eng Sci Med 2020;43:1049–67.

96. Bahaz M, Benzid R. Efficient algorithm for baseline wander and powerline noise removal from ECG signals based on discrete Fourier series. Australas Phys Eng Sci Med 2018;41:143–60.
97. Homaeinezhad MR, Ghaffari A, Atyabi SA. Design of a unified framework for analyzing long-duration ambulatory ECG: application for extracting QRS geometrical features. Biomed Eng Lett 2011;1: 116–28.
98. Sharma T, Sharma KK. A new method for QRS detection in ECG signals using QRS-preserving filtering techniques. Biomed Eng/Biomed Tech 2018;63:207–17.
99. Berkaya SK, Uysal AK, Gunal ES, Ergin S, Gunal S, Gulmezoglu MB. A survey on ECG analysis. Biomed Signal Process Control 2018;43: 216–35.
100. Gupta V, Mittal M, Mittal V, Saxena NK. A critical review of feature extraction techniques for ECG signal analysis. J Inst Eng (India): B 2021; 102:1049–60.
101. Crippa P, Curzi A, Falaschetti L, Turchetti C. Multi-class ECG beat classification based on a Gaussian mixture model of Karhunen-loève transform. Int J Simulat Syst Sci Technol 2015;16:1–2.
102. Jalal A, Batool M, Ud Din Tahir SB. Markerless sensors for physical health monitoring system using ECG and GMM feature extraction. In 2021 International Bhurban conference on applied sciences and technologies (IBCAST); 2021:340–5.
103. Zhong J, Hai D, Cheng J, Jiao C, Gou S, Liu Y, et al. Convolutional autoencoding and Gaussian mixture clustering for unsupervised beat-to-beat heart rate estimation of electrocardiograms from wearable sensors. Sensors 2021;21:7163.
104. Giri D, Acharya UR, Martis RJ, Sree SV, Lim TC, VI TA, et al. Automated diagnosis of coronary artery disease affected patients using LDA, PCA, ICA and discrete wavelet transform. Knowl Base Syst 2013;37: 274–82.
105. Martis RJ, Acharya UR, Prasad H, Chua CK, Lim CM. Automated detection of atrial fibrillation using Bayesian paradigm. Knowl Base Syst 2013;54:269–75.
106. Martis RJ, Krishnan MM, Chakraborty C, Pal S, Sarkar D, Mandana KM, et al. Automated screening of arrhythmia using wavelet based machine learning techniques. J Med Syst 2012;36:677–88.
107. Ghaffari A, Homaeinezhad MR, Daevaeiha MM. High resolution ambulatory holter ECG events detection-delineation via modified multi-lead wavelet-based features analysis: detection and quantification of heart rate turbulence. Expert Syst Appl 2011;38: 5299–310.
108. Rai HM, Chatterjee K. Hybrid CNN-LSTM deep learning model and ensemble technique for automatic detection of myocardial infarction using big ECG data. Appl Intell 2022;52:5366–84.
109. Liu B, Liu J, Wang G, Huang K, Li F, Zheng Y, et al. A novel electrocardiogram parameterization algorithm and its application in myocardial infarction detection. Comput Biol Med 2015;61:178–84.
110. Bentes PCL, Nadal J. A telediagnosis assistance system for multiple-lead electrocardiography. Phys Eng Sci Med 2021;44:473–85.